

CARBON DEPOSIT FORMATION FROM THERMAL STRESSING OF PETROLEUM FUELS

Orhan Altin and Semih Eser

Department of Energy and Geo-Environmental Engineering and The
Energy Institute
101 Hosler Building
The Pennsylvania State University
University Park, PA, 16802

Introduction

The thermal stability of fuels is of concern for the maintenance of all types of combustion engines. Thermal stability is measured in terms of the fuel's tendency to form deposits on fuel lines and nozzles of jet engines as well as on intake valves, fuel injectors, and combustion chamber surfaces in gasoline and diesel engines. Fuel degradation can cause engine failure, engine malfunction, and affects engine performance. Poor stability of fuel can lead to increased maintenance costs, and maintenance problems, such as equipment vulnerability and decreased reliability which may result in profit losses.

This article covers thermal decomposition of diesel fuel, gasoline, and jet fuel, and their respective reactions on metal surfaces leading to the deposition of carbonaceous solids.

Petroleum Fuels

Petroleum fuels, such as gasoline, diesel, and jet fuel contain a complex mixture of hundreds of hydrocarbons. The hydrocarbons vary by class—paraffins, olefins, and aromatics, depending on the nature of chemical bonding between the carbon atoms in hydrocarbon molecules. These fuels also contain additives designed for specific purposes. The molecular composition of fuels determines their physical properties, engine performance, and thermal stability characteristics. In general, fuels are produced to meet the property limits dictated by the industrial specifications and regulations, not to achieve a specific distribution of hydrocarbons by class, or size. Figure 1 shows a carbon number distribution of typical gasoline, which is in the range of C₄ to C₁₂ with the average carbon number of C_{6.8}. Gasoline also contains small amounts – less than 0.1 volume % – of heteroatom compounds with sulfur, nitrogen, or oxygen atoms (excluding added oxygenates) in their structures. Compared to gasoline, typical diesel fuel consists of a more complex mixture of thousands of individual compounds, most with carbon numbers between 10 and 22. Most of these compounds are members of the paraffins group (normal-, iso-, or cyclo-paraffins), or aromatic hydrocarbons boiling between approximately 150°C and 400°C. Originally diesel fuels were straight-run products obtained from crude distillation in a refinery. Today, where the demand for high-octane number gasolines and distillate fuels are high, diesel fuels may also contain distillates from cracking processes, such as light cycle oils (LCO) from Fluid Catalytic Cracking (FCC) unit.

Jet fuels (military and civilian turbine fuels, JP-5, JPTS, JP-7, JP-8, JP8+100, Jet-A, and Jet A-1) are mainly kerosene type having a carbon number distribution between about 8 and 16 carbon numbers, as seen in Figure 1. Kerosene fuels like JP-8 (military) or Jet A (civil) also contain a mixture of literally thousands of hydrocarbons. For JP-8, these hydrocarbons can be divided into three broad classes—aromatics (about 20%), n-paraffins and isoparaffins (60%), and cycloparaffins (naphthenes, 20%). Typically, normal paraffins have the highest concentration among the hydrocarbons and cycloparaffins and aromatics consist mostly of methyl-substituted single-ring molecules. The concentration of various components can

vary significantly from one batch to another, depending on the crude oil used and the process history of the fuels.

Problem of Thermal Stability

Thermal stability is typically described in terms of the fuel's tendency to form deposits on fuel lines, valves, injectors, and combustion chamber surfaces in engines. These fuel system deposits can be created by two distinct free radical pathways: low temperature autoxidation—usually called fouling—and higher temperature pyrolysis, called coking or carbon deposition.

Autoxidation or oxidative stability differs from thermal stability by referring to the rate at which oxygen is consumed and oxidative products are formed. Autoxidation reactions occur during fuel storage and exposure to high temperature in fuel lines which results in a series of liquid oxidation reactions of alkyl radicals generating hydroperoxides and other oxidized products which are believed to be responsible for solid deposit formation (1-4).

At elevated temperatures (>350°C), carbon deposits usually form via two different routes: Decomposition of hydrocarbons to elemental carbon and hydrogen; or polymerization/condensation of hydrocarbon species to larger polynuclear aromatic hydrocarbons (PAHs) which then nucleate and grow to become carbonaceous deposit. Metal catalysis of carbon deposition often follows the decomposition route, whereas non-catalytic (or thermal) carbon deposition usually proceeds via the polymerization route.

The formation of catalytic or non-catalytic carbon deposit depends on the characteristics of the substrate surface. A non-catalytic surface may affect the heat/mass transfer in the system and act as an inert substrate to collect the carbon deposit the formation of which is thermally initiated in the fluid phase. In contrast, a catalytic surface could, in addition, interact with the reactive species and accelerate the deposit formation.

Carbon Deposit Formation on Metal Surfaces During Thermal Stressing

Gasoline Fuel. Almost all types of gasolines produce carbon deposits on engine components over time. The rate of deposit formation depends on the nature of metal surfaces in the fuel systems and gasoline additives used to inhibit solid deposition. Carbon deposits mainly build up on fuel injectors, intake valves and ports, and in the combustion chamber. Fuel injectors are designed accurately meter fuel to the engine and deliver it in a precise pattern of fine droplets. Since the fuel passages are small, injectors are highly sensitive to small amounts of deposits in the critical regions where the fuel is metered and atomized. These deposits can reduce the fuel flow and alter the spray pattern, degrading driveability, decreasing power and fuel economy and increasing emissions. Deposit formation can cause similar problems in carbureted engines because carburetors also use a number of small channels and orifices to meter the fuel.

Problems with solid deposition in the combustion chamber and or in the intake system can sometimes be underestimated during initial engine development. Often, these problems become apparent after long duration of engine running time. Deposit precursors in the fuel delivery, or combustion units are formed by thermal cracking, oxidation, and polymerization of the fuel, and these processes may be catalyzed by metal surfaces.

Numerous investigations have suggested some possibilities for reducing these problems in the future. For example, Aradi et al. (5) investigated the role of surface catalytic activity in injector deposit formation and observed that in the presence of stainless steel walls greater amount of insoluble materials formed on the surface than that on a glass insert. Guthrie (6), on the other hand, found that the surface temperature was the most important factor in the formation of

deposits. Similarly, Kinoshita et al. (7) suggested that the best solution for deposit control was to use an insulating material on the areas of the injector exposed to the combustion chamber so as to raise the surface temperature to levels high enough to prevent deposit formation, i.e., 350°C, through oxidation/gasification of deposits, or deposit precursors

Deposit formation in gasoline engines appears to depend strongly on the chemical composition of high-boiling components of gasoline that have high deposition tendencies. Charlisle et al. (8) studied the effect of fuel composition on air-assisted direct injection spark ignition research engine and concluded that the aromatic hydrocarbon content of the fuel has a significant effect on deposit formation, higher the aromatics content more extensive was the deposit formation. The fuel olefin content, however, showed a less significant effect on deposit formation.

Intake valves and ports are subject to more deposit build up than fuel injectors because they operate at higher temperatures. Heavy valve and port deposits reduce maximum engine power because they restrict air flow. Intake valve deposits have also been shown to affect exhaust emissions, particularly VOCs and NOx. The engine deposits could cause substantial increase in exhaust gas temperatures, and therefore the octane number requirement because of preheating of the charge drawn into the cylinder. The increased octane number requirement prevents the use of optimum compression ratio and ignition timing, and consequently limits the engine efficiency well below the maximum possible with a fuel of a given octane number used in a clean engine.

Diesel Fuel. Diesel fuels can form deposits in the nozzle area of injectors that is exposed to high cylinder temperatures. The extent of deposit formation varies with engine design, fuel composition, lubricant composition, and operating conditions. Excessive deposit accumulation affects the injector flow patterns which, in turn, hinders the fuel-air mixing process that results in decreased fuel economy and increased emissions of soot and unburned fuel. To avoid the deposit formation problems on fuel injectors, detergent type additives are added to the fuel to keep the injectors clean. These additives are composed of a polar group that bonds to deposits and deposit precursors, and a non-polar group that dissolves in the fuel. Thus, the additive can redissolve deposits that already have formed and reduce the formation of deposits by stabilizing the deposit precursors.

Carbon deposit formation from diesel fuels mainly involves the chemical conversion of precursors to species of higher molecular weight with limited fuel instability. The precursors include nitrogen and sulfur containing compounds, organic acids, and reactive olefins. Pedley et al. (1) established a mechanism by which insolubles are formed in the acid-catalyzed conversion of phenalenones and indoles to complex indolylphenalene salts. Phenalenones are formed by oxidation of certain reactive olefins; indoles occur naturally in certain blend components of diesel fuel. Certain dissolved metals, especially copper, contribute by catalyzing oxidation reactions.

Thermal stability of diesel fuels is important because of their function as heat transfer fluid. More stringent thermal stability requirements may be necessary for future injector designs that employ higher pressures to achieve better combustion and lower emissions. Spilners and Hedenburg (9) who studied carbon deposit formation in single cylinder test engine observed that the olefin content of the fuel had the greatest effect on the deposit formation tendency.

Fuel injectors in diesel engines are precision instruments. Their function is to measure exactly the right amount of fuel into the combustion chamber on each compression stroke, to control engine combustion, fuel economy, and engine noise. Injector carbon deposits cause operational problems, such as excessive smoke emission, loss of power, poor fuel economy, degraded emission,

excessive engine noise, rough engine operation, and poor drivability. Injector carbon deposits, that usually appear as a lacquer on the piston that squirts the fuel through the injector nozzle, are believed to result from the reactions of the oxidation products of unstable diesel fuel (10).

Jet Fuel. Recent advances in jet aircraft and engine technology have placed an ever-increasing heat load on the aircraft. Currently, jet fuels play two important roles in advanced aircraft, propellant and coolant. The need to cool hot parts of the engine had been evident ever since the invention of the internal combustion engine. As engine performance goals and flight speeds have increased, the need for more effective cooling has also increased. For example, the thermal stability limit of JP-8 fuel was established at a bulk temperature of 163°C and a wetted wall temperature of 204°C. Exposure to higher temperatures accelerates the fuels reactions that lead to gum and carbon deposit accumulation in: i) fuel filters, increasing the pressure drop across the filter and reducing fuel flow, ii) fuel injector nozzles, disrupting the spray pattern, which may lead to hot spots in the combustion chamber, iii) the main engine control, interfering with fuel flow and engine system control, and iv) heat exchangers, reducing heat transfer efficiency and fuel flow. These deposits may lead to increased maintenance and in extreme cases, to disastrous accidents. To resolve the problem, an Aircraft Thermal management Working Group of Wright Research and Development Center (WRDC) recommended the development of high thermally stability fuels, such as: (i) a high temperature thermally stable JP-8+100 fuel which provides a 50% improvement in the heat sink capability over conventional JP-8 fuel, and (ii) a new fuel JP-900 that has a 482°C thermal stability and could eliminate the need to recirculate fuel onboard an aircraft. To meet the evolving challenge of improving the cooling potential of jet fuel, while maintaining the current availability at minimal cost a joint government/industry/academia program developed an additive package for JP-8 fuel named as JP8+100 fuel. Hundreds of additives have been tested and a package has been formulated that contains a detergent/dispersant in addition to the standard antioxidant and metal deactivator additives. The additive package allows the bulk fuel temperature to increase from 163°C to 218°C without generating fuel system deposits (11).

Marteny and Spadaccini (12) suggested two basic coking processes: 1) A homogeneous oxidation reaction occurring in the fuel free stream forming coke particles which adhere to the fuel passage surface. 2) A heterogeneous catalytic reaction occurring at the fuel passage metal surface. If mechanism #1 dominates, a polished surface may prevent carbon from adhering. If, on the other hand, mechanism #2 dominates, an inert surface should reduce the coking rate.

Metal surfaces could act as catalysts for dehydrogenation reactions that lead to the formation of carbon deposits. At elevated temperatures, stainless steel surfaces deposit large amounts of carbonaceous deposits from jet fuel decomposition. Carbon deposit precursors such as radicals and unsaturated hydrocarbons are formed in the gas phase and react with active centers on metal surfaces (13,14) An effective way of preventing deposition from pyrolysis of fuels was found to be the use of inert coatings such as Zirconia (15) and Silcosteel® (Restek Corp, State College, PA) (14). Coating of metal alloy surfaces prevents interaction between deposit precursors and active metal surfaces that lead eventually to deposition of solid carbon.

Trace amounts of some sulfur compounds may also affect the rate of deposit formation and metal surface degradation. The sulphidation of metals at high temperatures has become a matter of increasing concern in industrial applications, particularly in energy conversion systems using fossil fuel. Because of high diffusivity and formation of eutectic melts with metals, sulfur reacts with metals to

form metal sulfides at relatively low temperatures, causing severe localized corrosion on heat-resistant alloys and superalloys. Taylor (16) examined the role of sulfur compounds in deposit formation from a JP-5 fuel. Addition of 300 ppm diphenyl sulfide and phenyl benzyl sulfide to JP-5 fuel enhanced the carbon deposit formation significantly. On the other hand, addition of benzothiophene and dibenzothiophene did not contribute to the formation of deposits. Figure 2 summarizes the carbon deposit formation mechanism on metal surfaces by combining hydrocarbon degradation on catalytic metal surface with sulfur-metal reaction resulting in amorphous and filamentous carbon deposition.

Conclusions

The long-term automotive and aircraft related technological benefits can be derived from fundamental understanding of fuel thermal stability issues such as, free radical autoxidation mechanism, establishing a global chemistry model, understanding of fuel-metal surface interactions, and developing additive packages to increase the thermal stability of gasoline, diesel, and jet fuels. Research and development efforts in these areas will help eliminate the operational problems associated with carbon deposit accumulation on various components of fuel delivery and combustion systems in internal combustion engines.

References

- (1) Pedley, J. F.; Hiley, R. W.; Solly R. K., *Fuel*, 1989, 68, 27-31.
- (2) Zabarnick, S., *Chem. Ind. Eng. Chem. Res.* **1993**, 32, 1012-1017.
- (3) Haneghan, P. S.; Zabarnick, S., *Fuel*, **1994**, 73, 35-43.
- (4) Edwards, T.; Zabarnick, S., *Ind. Eng. Chem. Res.* **1993**, 32, 3117-3122.
- (5) Aradi, A. A.; Imoehl, B.; N. L. Avery, N. L.; Wells, P. P.; R. W. Grosser, R. W., SAE Paper, 1999-01-3690.
- (6) Guthrie, P. W., SAE Paper, 2001-01-1202.
- (7) Kinoshita, M.; Narasimhan, S.; Shibata H.; Niwa Y., European Patent EP0828075, 1998.
- (8) Charlisle, H. W.; Frew, R. W.; Mills, J. R.; Aradi, A. A.; Avery, N. L., SAE Paper 2001-01-2030.
- (9) Spilners, I. J.; Hedenburg J. F., In *Chemistry of Engine Combustion Deposits*; Ebert, L. B., Ed.; Plenum Press, New York, 1985; 289.
- (10) Sapienza, R. S.; Butcher, T.; Krushna, C. R.; Gaffney, J., In *Chemistry of Engine Combustion Deposits*; Ebert, L. B., Ed.; Plenum Press: New York, 1985; 263-272.
- (11) Haneghan, S. P.; Zabarnick, S.; Ballal, D. R.; Harrison, W. E., 34th Aerospace Sciences Meeting and Exhibit, Reno, NV, Jan 15-18, 1996; AIAA 96-0403.
- (12) Marteney, P. J.; Spadaccini, L. J., *J. Eng. Gas Turb. Pow. (ASME Transactions)*. **1986**, 108, 648-654.
- (13) Altin, O.; Eser, S., *Ind. Eng. Chem. Res.* **2001**, 40, 596-603
- (14) Altin, O.; Eser, S., *Ind. Eng. Chem. Res.* **2001**, 40, 589-595.
- (15) Sticles, R. W.; Dodds W. J.; Koblish T. R.; Sager J.; Clouser S., *J. Eng. Gas Turb. Pow. (ASME Transactions)*. **1993**, 115, 439-447.
- (16) Taylor, W. F., *Ind. Eng. Chem. Prod. Res. Dev.* **1976**, 15, 64-68.

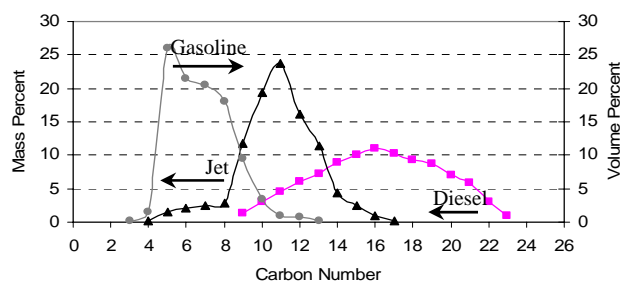


Figure 1. Carbon number distribution of petroleum fuels.

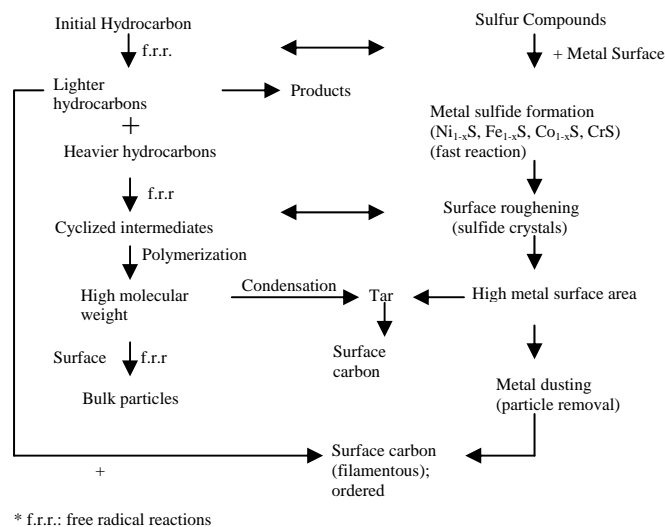


Figure 2. Carbon deposition mechanism including sulfur-metal surface involvement.

CHARACTERIZATION OF DIESEL AND BIODIESEL SOOT

Juhun Song, Mahabubul Alam and André L. Boehman

The Energy Institute
The Pennsylvania State University
405 Academic Activities Building
University Park, PA 16802

Kirk Miller

ConocoPhillips
600 N. Dairy Ashford
Houston, TX 77252

Introduction

Diesel fuel production from renewable sources such as vegetable oils and animal fats offers the potential of both reducing fossil carbon emissions and producing alternative ultra clean transportation fuels. It is well known that biodiesel, neat or in blends, can provide reductions in PM mass emission through either oxygen content or enhanced air entrainment due to the higher boiling range of biodiesel [1]. However, recent observations have indicated that biodiesel may provide other benefits with regard to particulate emissions. These observations have shown an oxidation reactivity variation with soots derived from different fuels. Identifying the dominant mechanism during oxidation, if any, may have practical implications for reducing the temperature required to regenerate catalyzed diesel particulate filter (DPF) [2-3]. There exists evidence of correlation between reactivity and structure in the case of carbon blacks or coal chars that are synthesized from different hydrocarbons and at different temperature conditions [4-5]. However, the manner in which crystallinity or pore structure affects soot oxidation rates has not been clarified for diesel soot whether that soot is derived from conventional or alternative fuel sources.

In this paper, we present comparison of soot nanostructures of particulates produced from two different fuels (an ultra low sulfur diesel fuel and its B20 blend) on commercial direct injection (DI) diesel engine by means of high resolution electron microscopy imaging. This crystalline information such as the graphene layer size and orientation is used to interpret the quantitative reactivity difference measured in an idealized TGA/DSC oxidation experiment. Together, these results show the potential impact of biodiesel blending on the low temperature oxidation characteristics of soot.

Experimental

PM Production and Sampling. A highly instrumented 6-cylinder Cummins ISB 5.9L DI turbodiesel engine, connected to a 250 HP eddy current dynamometer, was used to produce different particulate samples at a fixed engine operating condition (2700 rpm and 25% load of peak). The engine has been heavily instrumented with a 0.1 crank angle resolution crank shaft encoder, a cylinder pressure sensor and a needle lift sensor. The engine and dynamometer are operated through an automated control system. To isolate any effect of cylinder temperature history from possible changes in soot nanostructure due to differences in the fuels, the time evolution of in-cylinder mean temperature was obtained through cylinder pressure trace analysis, along with consideration of injection timing and cylinder geometry. Two test fuels were considered, an ultra low sulfur diesel with 15 ppm sulfur content, BP15, and a B20 blend (e.g., a blend of 20 wt.% methyl esters in BP15 fuel). Some fuel properties are provided in Table 1. For TPO test, bulk samples were collected in quartz filters from diluted exhaust gas via a mini-

dilution tunnel (Sierra Instruments BG-1). Then, the filter was crushed into a powder and 10 mg of the powder was evenly deposited into the sample pan in the furnace. For HRTEM imaging, thermophoretic sampling was used to capture PM from the raw exhaust. For imaging of the partially oxidized samples, an acoustic suspension in ethanol was used to disperse the sample onto a TEM carbon grid.

Table 1. Properties for Ultra Low Sulfur Diesel and its B20 blend

Fuels	Sulfur Content, ppm	Oxygen Content, wt.%	Cetane Number
BP-15 ULSD	15	0	50.5
B20 Blend	13	2	52.5

Particulate Reactivity. The temperature programmed oxidation (TPO) is examined in two different laboratory reactors as a means of evaluating the differences in reactivity of the soot samples. All particulate samples were treated by 30 minutes heating at 500 °C under inert gas (i.e. argon) in the TGA to eliminate the soluble organic fraction (SOF). Then, samples were subjected to slow heating to obtain the burning rate of each sample on both DSC (TA2920) and TGA (PE-TGA7). This pretreatment for SOF removal has been reported to yield the same effect as post extraction with dichloromethane (CH₂Cl₂) [6]. Ignition temperature was used to determine the oxidation reactivity of the samples. From the mass loss curve from the TGA, ignition temperature is determined as the temperature at which soot starts oxidizing at an appreciable rate. A detection of heat release by DSC was used as a supplement to gauge the ignition temperature of different particulate samples [7]. In this DSC configuration, the ignition temperature is determined by thermal runaway that is controlled by competition between heat of combustion and heat loss to gas flow.

Soot Nanostructure Imaging. Structural properties of the diesel particulates were obtained by electron beam probes. Among several characterization techniques to detect the degree of crystallinity of graphene layer, a bright field image method by high-resolution transmission electron microscopy (HRTEM) was employed on field emission JOEL 2010F operated on 200 kV, with a point to point resolution of 0.23 nm. In bright field image mode, graphene layer segments are observed as the dark lines blocking/scattering the incident electron beam, thereby creating a dark image on the screen. A thin isolated particle deposited a perforated carbon film is used to obtain the sharp phase contrast while minimizing the interference with the condensable fraction and the grid substrate, since the existence of adsorbed hydrocarbon may block the high contrast imaging of the carbon-rich dry soot.

Results and Discussion

Particulate Reactivity. Figure 1(a) compares from mass loss curve of TGA while Figure 1 (b) compares heat release curve of DSC, both of which indicate the differences in the ignition temperature of the soot samples. Compared to BP15 diesel soot, the B20 soot exhibits a lower ignition temperature by 40~50 °C in both the burning rate curve by DSC and mass reduction by TGA.

Soot Nanostructure. Results from HRTEM imaging are shown in Figures 2a-d. The figures compare the soot nanostructure for the BP15 and B20 soot at two different oxidation stages, shown in terms of burn off time. From the comparison between BP15 soot and B20 soot at the initial stage (no burn-off), a more amorphous and disordered arrangement of short-range graphene segments is apparent for the B20 soot as shown in Figures 2a and 2b.

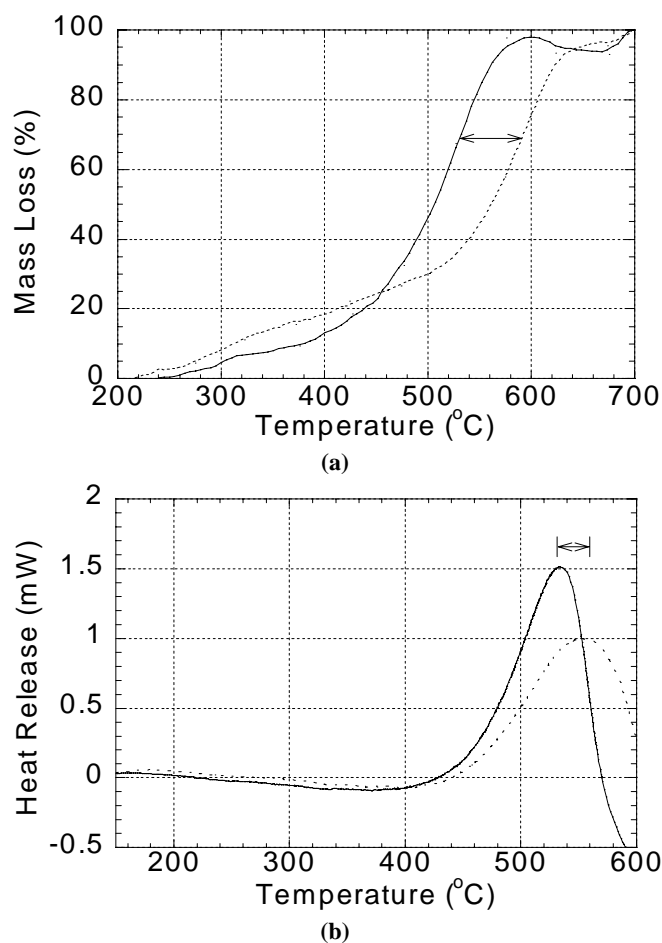


Figure 1. (a) Mass reduction TGA curve of pretreated samples under 21% oxygen; (b) DSC burning rate of pretreated samples under 21% oxygen. Treated sample is prepared by 30 minutes heating at 500 °C under inert argon. (---) BP15 soot and (—) B20 soot.

Within this primary particle from the B20 soot, wrinkled or curved crystallites with many misalignments relative to each other and structural defects are more pronounced. In contrast, BP15 diesel soot possesses typical the shell-core structure in which graphene layers are oriented parallel to external outer surface, but are randomly oriented in a central core. The more reactive edge site carbon, which is more prevalent with short-range amorphous arrangement of the crystallites, is known to be more vulnerable to oxidative attack due to greater accessibility and electronic affinity for O₂ chemisorption [4,5]. Consistent with this understanding of the relationship between structure and oxidative activity, B20 soot indeed leads to higher reactivity compared to the BP15 soot partly due to differences in soot nanostructure.

The partially oxidized samples shown in Figures 2c and 2d display nanostructural changes after exposure to 500°C for 30 minutes. The BP15 soot, that has initially a shell-core structure, remains untouched or slightly graphitized, indicating slow surface burning progression during the course of oxidation. On the contrary, for the B20 soot, porous and ragged layers have developed, indicating a faster burning through either internal burning or stripping of the outer crystallite structure. Although few if any studies have compared the microstructural variations during oxidation for soots derived from different fuels, the observations in this work are consistent with the reported progression of soot

oxidation wherein more surface area was developed through opening of micropores by removal of adsorbed hydrocarbon, followed by pre-graphitization before the outer crystallite is stripped away at greater extent of burn-off [8-9]. Consistent with the quantitative measures in Figure 1, this qualitative comparison of nanostructure between the partially oxidized samples supports a significant difference in reactivity.

Although identifying the dependence of soot nanostructure on the conditions during soot formation is not the main objective of the present work, a preliminary hypothesis can be offered to explain the amorphous soot structure observed with biodiesel addition, related to effects of Biodiesel on the combustion process and affecting soot formation. Due to the effect of temperature and its time variation on the extent of carbonization of soot, variation in soot nanostructure and soot oxidation rate is known to exist between mature soot and soot precursor particles that are not yet fully carbonized [10]. As seen in Figure 3, comparison of temperature-time history (regarding the length of time that soot precursor particles experience various temperatures after soot inception and through the carbonization period) shows that there is no significant difference between the two fuels in terms of temperature-time history during ignition and the premixed burn period, during which time changes in temperature could have altered soot inception and growth.

Therefore, other factors, most likely related to fuel composition and its decomposition chemistry, are likely to be responsible for the more amorphous structure in the B20 soot. Based upon calculations of the evolution of equilibrium soot structures [11], when insufficient PAH is available during the soot inception period to attain the threshold mass requirement, a soot particle will not transition into the ordered morphology of the typical shell-core structure. Differences in the soot growth mechanism, caused by different soot growth species formed during the fuel decomposition period may also lead to differences in structure, as hypothesized and verified in recent work by Vander Wal and Tomasek. [12]. While formation of heavy PAH species leads to an amorphous structure through the coalescence growth mechanism, light acetylene (C₂H₂) addition on the radical sites of PAH species leads to formation of graphitic structures through the HACA (Hydrogen Abstraction Carbon Addition) mechanism. The coalescence growth mechanism may be more pronounced for combustion and soot growth conditions with the B20 fuel, leading to a more amorphous soot nanostructure.

Conclusions

With B20 fuel, soot exhibits higher oxidative reactivity in DSC/TGA tests. A more short-range, amorphous structure in the B20 soot is partly responsible for its enhanced reactivity. However, other effects arising from internal pore structure or surface functional group on soot oxidation remain to be investigated.

Acknowledgement. The authors wish to thank Etop Esen, Doug Smith, Keith Lawson, Ed Casey, Rafael Espinoza and Jim Rockwell of ConocoPhillips, and John Wright and Edward Lyford-Pike of Cummins Engine Company for their support of this work. This work is a part of ongoing Ultra Clean Fuels project entitled "Ultra Clean Fuels from Natural Gas," sponsored by U.S. Department of Energy under Cooperative Agreement No. DE-FC26-01NT41098.

The Government reserves for itself and others acting on its behalf a royalty-free, nonexclusive, irrevocable, worldwide license for Governmental purposes to publish, distribute, translate, duplicate, exhibit, and perform this copyrighted paper. High Resolution Transmission electron microscopy was performed using the facilities of the Materials Research Institute at The Pennsylvania State University and the authors are grateful for access to these facilities.

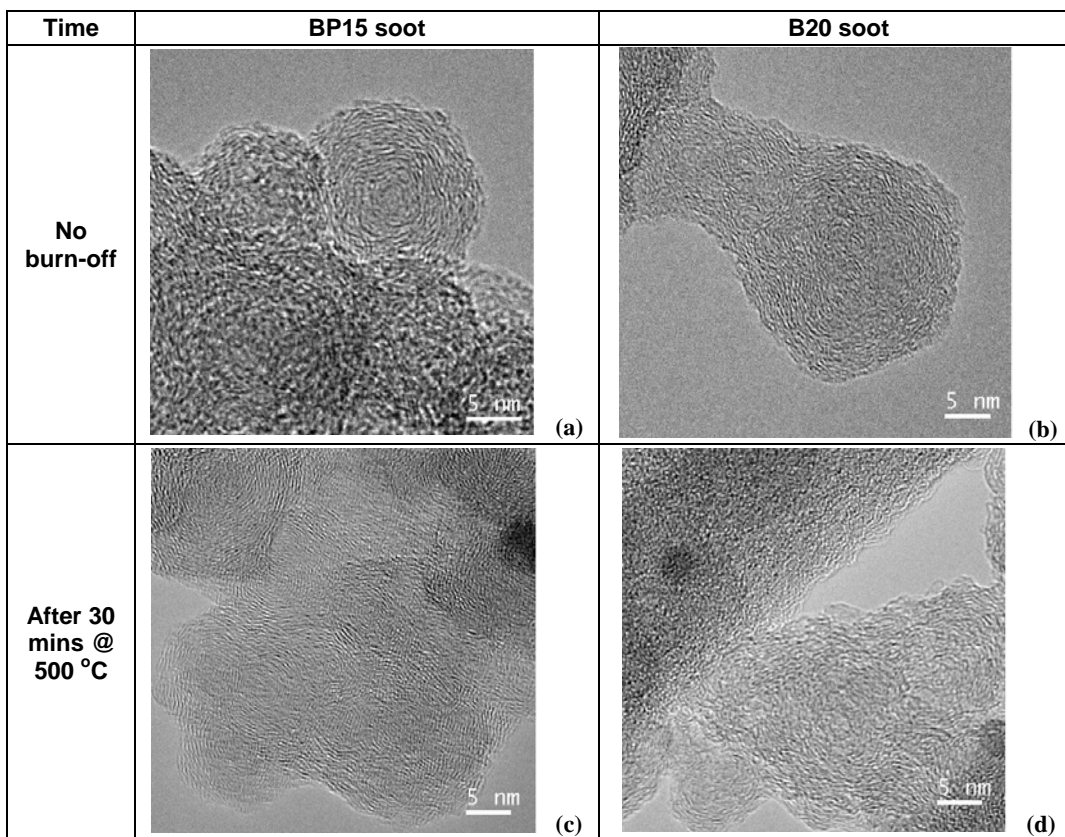


Figure 2. HRTEM images of BP15 diesel and its B20 soot at two different stages of oxidation

This material was also prepared with the support of the Pennsylvania Department of Environmental Protection. Any opinions, findings, conclusions, or recommendations expressed herein are those of the author(s) and do not necessarily reflect the views of the DEP.

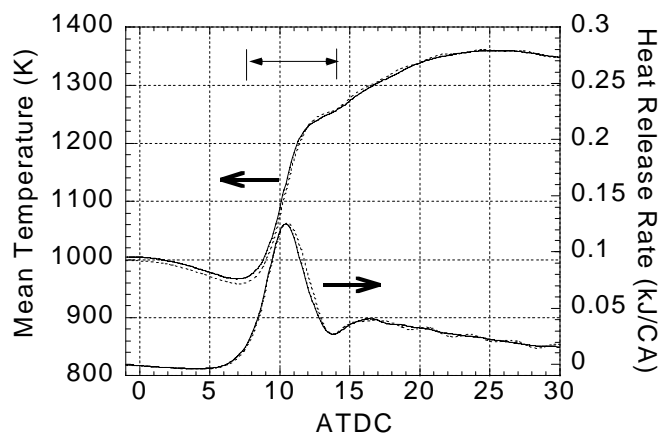


Figure 3. Time evolution of in cylinder mean gas temperature during ignition and premixed burn period of diesel combustion process leading to soot inception and growth. (---) BP15 fuel and (—) B20 fuel.

References

- [1] Graboski, M.S. and McCormick, R.L., "Combustion of Fat and Vegetable Oil Derived Fuels in Diesel Engines", *Prog. in Energy and Comb. Sci.*, Vol.24, p.125-164, 1998.
- [2] Allanson, R., Blakeman P.G., Cooper, B.J., Howard, H., Silcock, P.J. and Walker, A.P., "Optimizing the Low Temperature Performance and Regeneration Efficiency of the Continuously Regenerating Diesel Particulate Filter(CR-DPF) System", SAE 2002-01-0428, 2002.
- [3] Stanmore, B.R., Brilhac, J.F. and Gilot, P., "The Oxidation of Soot: A Review of Experiments, Mechanisms and Models", *Carbon*, Vol. 39, p.2247-2268, 2001.
- [4] Vander Wal, R.L. and Tomasek, A.J., "Soot Oxidation: Dependence upon initial nanostructure", *Comb. and Flame*, Vol. 132, 2003.
- [5] Marsh, H., "Kinetics and catalysis of carbon gasification", in: *Introduction to Carbon Science*, p.107-152, Butterworths, London, 1989.
- [6] Stratakis, G.A. and Stamatelos, A.M., "Thermogravimetric Analysis of Soot Emitted by a Modern Diesel Engine Run on Catalyst-Doped Fuel", *Comb. and Flame*, Vol. 132, p.157-169, 2003.
- [7] Neef, J.P.A., Nijhuis, X., Smakman, E., Makkee, M. and Moulijn, J.A., "Kinetics of the Oxidation of Diesel Soot", *Fuel*, Vol. 76, p.1129-1136, 1997.
- [8] Ishiguro, T., Suzuki, N., Fujitani, Y. and Morimoto, H., "Microstructural Changes of Diesel Soot During Oxidation", *Comb. and Flame*, Vol.85, p 1-6, 1991.
- [9] Palotas, A.B., Rainey, L.C., Sarofim, A.F., Sande, J.B.V., Ciambelli, P., "Effect of Oxidation on the Microstructure of Carbon Blacks", *Energy & Fuels*, Vol. 10, p.254-259, 1996.
- [10] Chen, H.X. and Dobbins, R.A., "Crystallogensis of Particles Formed in Hydrocarbon Combustion", *Comb. Sci. and Tech.*, Vol.159, p.109-128, 2000.
- [11] Hurt, R.H., Crawford, G.P. and Shim, H.S., "Equilibrium Nanostructure of Primary Soot Particles", *Proc. of the Combustion Institute*, Vol. 28, p.2539-2546, 2000.
- [12] Vander Wal, R.L. and Tomasek, A.J., "Soot Nanostructure: Dependence upon Synthesis Conditions", *Comb. and Flame*, Vol. 136, p. 129-140, 2004

THE EFFECT OF CHEMICAL COMPOSITION OF COAL-DERIVED JET FUELS ON CARBON DEPOSITS

Leslie R. Rudnick, Ömer Gül, Harold H. Schobert

The Energy Institute,
C205 Coal Utilization Laboratory
The Pennsylvania State University,
University Park, Pennsylvania 16802

Introduction

Thermal stability of aviation jet fuel refers to its resistance to decomposition at elevated temperatures to form deleterious solid deposits.

The carbonaceous deposits formation on metallic surfaces from thermal decomposition of jet fuels is a major concern in the development of high-speed aircraft in which the fuel is presently used as a coolant, in addition to its primary use as a propellant. It is used to cool the lubrication system, avionics, electrical systems and environmental control systems, and is also used as a hydraulic fluid (1). The jet fuel instability has been studied for almost five decades (2-5). Solid deposits from fuel degradation can attach to the surface of the flow lines or plug filters and create problems with the fuel system operation. The carbonaceous deposit formation appears to depend on a combination of different conditions, such as the reactivity of the starting fuel, the temperature, the pressure, the concentration, and the nature of the substrate surface. Various metallic alloy candidates were examined at Penn State to observe their catalytic activity in carbon deposit formation from jet fuel decomposition and found that Inconel X and Inconel 718 collected significantly less amount of deposit at 500 and 600°C during jet fuel stressing experiments (6-7).

Temperature is one of the most important parameters that affect the rate and reaction mechanisms of fuel degradation. Autooxidation of fuels takes place at temperatures less than 260°C, decomposition of oxygenated products at intermediate temperatures between 290 and 350°C, and pyrolysis at temperature greater than 350°C (8).

The composition of jet fuels is very complex. Many studies have been carried out with light hydrocarbons (9-13) to understand the mechanism of carbon formation on metals. One distinguishing property of carbon deposits is their oxidation reactivity, which depends on the chemical composition and the structure of the deposits. Differences in oxidation reactivity of the deposits are manifested in the evolution of CO₂ peaks at different temperatures during temperature-programmed oxidation (TPO) experiments (14,15). The TPO analysis is, therefore, useful to help understand the role of the metal surface in carbon deposit formation.

This study examines the thermal stability behavior of different severity hydrotreated of 1:1, 2:1 and 3:1 blends of refined chemical oil (RCO) with light cycle oil (LCO), and JP-8 on Inconel 718 surface at 470°C of fuel temperature in terms of carbon deposit amount.

Experimental

Thermal Stressing Experiments. The fuels tested in the thermal stressing experiments on Inconel 718 are coal-based blends HDT- (1:1 vol) RCO/LCO), HDT- (2:1 vol) RCO/LCO), HDT- (3:1 vol) RCO/LCO), and petroleum-based JP-8. The nominal composition of Inconel 718 alloy is (wt%) Ni:52.5, Fe:18.5, Cr:19, Mo:3.05, Al:0.5, Ti:0.9, Nb+Ta:5.13, Cu:0.15, Mn:0.18, Si:0.18, C:0.04, S:0.0008. The alloy foils, 15 cm x 3 mm x 0.6 mm, were cut and rinsed in acetone. Thermal stressing of fuels was carried

out at 470°C fuel temperature (500°C wall temperature) and 250 psig (17 atm) in the presence of Inconel 718 foil. The fuel was subjected to stressing for 5 hr at a 4 ml/min flow rate. The alloy foil was placed in the 26.5 cm and 1/4 in OD glass lined stainless steel tube reactor. The fuel was preheated to 200°C before entering the reactor. Throughout the experiments, the reactor outlet temperature, wall temperature, fuel pressure, and liquid fuel flow rate were kept at 470°C, 500°C, 17 atm., and 4 mL/min, respectively. The stainless steel preheating section is 2 mm in i.d. (1/8-in. o.d.) and 61 cm in length. The fuel residence time in this preheating zone is 22 sec. at a liquid fuel flow rate of 4 mL/min. The fuel residence time in the reactor (4 mm. i.d., 0.25 in. o.d. and 31.75 cm length) is 59 sec. at the same fuel flow rate. At the end of the reaction period (5 h.), the foils were cooled under an argon flow in the reactor. Details about the flow reactor system are reported (16).

Chemical composition of jet fuels before and after thermal stressing was determined by using GC/MS analysis. The total amount of carbon deposition on metal strips was determined using a LECO Multiphase Carbon Analyzer. The deposits formed on Inconel 718 surface were characterized by temperature-programmed oxidation (TPO).

Materials. Inconel 718 was obtained from Goodfellow Metals Ltd (Cambridge, U.K.)

Jet fuels used in thermal stressing were obtained from PARC. They were hydrotreated in different severity. To verify the reproducibility of the experimental results, duplicate experiments of jet fuel stressing were carried out with different jet fuel blends in the presence of Inconel 718. The results of duplicate experiments showed that the TPO profiles were reproducible with respect to individual peak positions and relative peak intensities. The total amount of deposition measured for different jet fuel blends were reproducible $\pm 10\%$ of the deposit mass.

Results and Discussion

In this study, relationships between carbon deposition and chemical composition of the jet fuel were sought, chemical compositions of original sample and thermally stressed fuel samples were determined with GC-MS.

The JP-8 fuel used in this study consists mainly of long-chain paraffins, with lower concentrations of alkyl cyclohexanes, alkyl benzenes, and alkyl naphthalenes (9). The coal derived-blends contained mostly tetralin, naphthalene, decalin and their alkyl substitutes, with lower concentration of paraffins, saturated cyclics, alkyl benzenes and indanes. Neither indene or its derivatives were observed.

Exposure of jet fuel to high temperatures in aircraft fuel lines triggers pyrolysis reactions that eventually lead to deposition of carbonaceous solids on metal surfaces. This is particularly important problem for advanced future aircraft which may expose fuel to very high temperatures.

A wide range of variation was observed in the amount of carbon deposits obtained from different blends. Table 1 shows the compositions of coal-derived jet fuel components: naphthalenes, tetralins, decalins in %, sulfur (ppm) and nitrogen (ppm), and carbon deposits produced from thermally stressing of fuels, reported in terms of micrograms of carbon deposit per square centimeter foil. The lowest and the highest carbon depositions were obtained with EI-082 and EI-103, respectively, among the 12 coal derived-blends and JP-8. The lowest carbon deposition amount was 4.08 $\mu\text{g}/\text{cm}^2$ with EI-082, and the highest carbon deposition amount was 33.62 $\mu\text{g}/\text{cm}^2$ with EI-103. This large difference in deposition tendency under the same stressing conditions can be attributed to

the differences in the chemical composition of fuels, and their S and N concentrations. EI-103 has the highest sulfur concentration and also it has the highest naphthalenes concentration among the tested fuels. EI-103 also has the lowest tetralins and decalins concentration as a result of lower severity hydrotreating conditions.

When all of the thermally stressed samples were taken in to consideration, no relationship was found between alkyl benzenes or indanes and carbon deposition.

All of the coal derived-blends contain 40% or higher amount of tetralins but the observed carbon deposit varied from blend to blend. One can conclude that, carbon deposition is independent of tetralins concentration when the tetralins concentration is 40% or higher. For example, if the first two 1:1 blends are compared, the carbon deposits are almost same but tetralins concentrations are different.

To assess the effect of chemical composition on carbon deposition relationships between chemical group concentration and deposits were plotted. A plot of saturated cyclics versus deposit for each blend ratio separately shows that carbon deposition increases as the saturated cyclic concentrations decreases. Saturated cyclics don't contain decalin or its derivatives and decalins were evaluated separately.

If decalin concentrations are plotted relative to carbon deposit, similar trends to that found for saturated cyclics is observed, e.g. as decalins concentrations decreases carbon deposit increases.

All of the blended jet fuels contain different amounts of tricyclic compounds (4.20 to 9.63%). Some of these have been identified as dibenzofuran, octahydro phenanthrene, octahydro anthracene, hexahydro fluorene, acenaphthene, and hexahydro acenaphthylene. Carbon deposition on metal coupon increased with increasing tricyclic compounds concentration in the blend. Due to their larger structure, and if they are exposed to severe conditions, they can form radical and further react to form larger molecule which can become carbonaceous materials which are not desired.

It can be seen from the GC-MS analysis of before and after thermal stressing samples that the component that decreased the greatest was naphthalene or its derivatives, while the tricyclic compounds concentration was increased. These molecules (naphthalenes, alkyl naphthalenes) thermally form radicals and further reaction of these molecules may produce higher molecular weight compounds leading to deposits.

Relatively high carbon deposition was obtained from thermal stressing of JP-8 (17.48 $\mu\text{g C/cm}^2$). This may also be explained by JP-8's chemical composition. JP-8 contains some alkene+alkyne (Table 1) which may also form radicals and result as initiators for the formation of carbonaceous materials. GC-MS analysis results on the JP-8 sample obtained after the thermal stressing experiment showed that there was about 25% decrease in their concentration.

Figure 1 shows the TPO profiles for the deposits of three fuels on the Inconel 718. This figure compares samples having the highest and lowest carbon deposits obtained from coal derived-blends and JP-8. The low temperature peaks around 150 and 350°C can be attributed to adsorbed liquids on the deposits and hydrogen-rich amorphous deposits, respectively. While the JP-8 and EI-082 had given broad and low-intensity relative-carbon signal band, EI-103 gave a sharp and narrow band in the TPO profile because of the significantly higher deposit. The most intense peak evolved at approximately 450°C for JP-8.

Conclusion

In this work it was found that jet fuels containing low sulfur and nitrogen and higher amount of decalins and saturated cyclics gave low carbon deposition at 470°C. Carbon deposition was found to be independent of RCO-LCO blend ratio.

Acknowledgement. Financial support for this work was provided by the U.S. Air Force Office of Scientific Research.

References

- (1) Zabarnick, S.: *Ind. Eng. Chem. Res.* **1994**, 33, 1348
Bol'shakov, G. F.; Technical Report; Wright-Paterson Air Force Base, Dayton, OH, **1972**
- (2) Schimdt, J. E.; Kirklin, P. W., David, P., Eds.; ASTM STP 1138; ASTM: Philadelphia, PA, **1992**
- (3) Heneghan, S. P.; Martel, C.R.; Williams, T.F.; Ballal, D. R. *Trans. ASME J. Eng. Gas Turbines Power* **1993**, 115, 480
- (4) Edwards, T.; Zabarnick, S. *Ind. Eng. Chem. Res.* **1993**, 32, 3117
- (5) Hunt, J. E.; Winans, R. E.; Ahrens, M.; and Xu, L. *Prepr. Pap. - Am. Chem. Soc., Div. Fuel Chem.*, **1999**, 44 (3), 610.
- (6) Altin, O.; Eser, S.; *Ind. Eng. Chem. Res.*, **2001**, 40, 589.
- (7) Elliot, P.; Hampton, A.F.; *Oxid. Met.*, **1980**, 14, 449.
- (8) Song, C.; Eser, S.; Schobert, H.H.; Hatcher, P.G. *Energy Fuels*. **1993**, 7(2), 234
- (9) Trimm, L.D. *Catal. Rev.-Sci. Eng.* **1977**, 16, 155
- (10) Trimm D.L.; Albright, L.F., Crynes, B.L., Corcoran, W.H., Eds.; Academic Press: New York, **1983**.
- (11) Baker, R.T.K.; Harris, P.S.; Walker P.L., Jr., Thrower, P.A., Eds.; Marcel Dekker Inc.: New York, **1978**.
- (12) Albright, L.F.; Tsai, C.-H.T.; Albright, L.F., Crynes, B.L., Corcoran, W.H., Eds.; Academic Press: New York, **1983**.
- (13) Froment, G.F. *Rev. Chem. Eng.* **1990**, 16(4), 293.
- (14) McCarty, J.G.; Wise, H. J. *Catal.* **1979**, 57, 406.
- (15) Marecot, P.; Akhachane, A.; Micheaud, C.; Barbier, J. *Deactivation by Coking of Supported Palladium Catalysts. Effect of Time and Temperature. Appl. Catal. A: Gen.* **1998**, 169, 189.
- (16) Altin, O.; Eser, S., *Ind. Eng. Chem. Res.* **2001**, 40, 596-603.

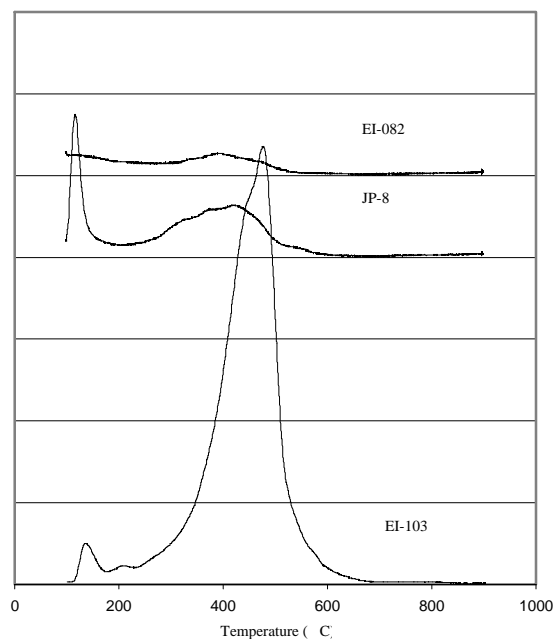


Figure 1. Selected TPO profiles of carbon deposits from thermal stressing of coal derived-blended fuels and JP-8 on Inconel 718 at 470 °C fuel temperature for 5h with 4 mL/min flow rate.

**Table 1. Total Carbon Deposit and Compositions of HDT Coal-Derived Jet Fuels (JP-900 prototypes):
Thermal Decomposition on Inconel 718 at 470 °C /17 atm (250 psig) / 5 h / 4 mL/min Flow Rate.**

Sample Code	Fuel Type	Paraffins %	Sat. Cyclics %	Alkyl Benzenes %	Indanes %	Naphthalenes %	Tetralins %	Decalins %	Tricyclic Comp.s %	Alkene+ Alkyne	Alkyl alcohols	S, ppm	N, ppm	C Deposit (ug C/cm ²)
	JP-8	73.50	7.31	9.27	-	2.70	0.25	0.05	-	4.20	2.72	na	Na	17.48
EI-072	1:1 RCO/LCO	1.1	0.51	4.08	3.25	19.97	62.34	0.57	8.19	-	-	160	967	15.06
EI-073	1:1 RCO/LCO	0.94	0.49	7.77	5.04	31.02	47.08	0.55	7.13	-	-	68	1500	15.78
EI-076	1:1 RCO/LCO	0.96	0.60	6.17	5.17	31.75	48.2	0.39	6.75	-	-	23	205	7.21
EI-079	1:1 RCO/LCO	1.47	2.78	7.65	4.56	4.19	66.58	5.59	7.19	-	-	61	16	11.52
EI-082	1:1 RCO/LCO	0.79	7.73	7.22	3.39	4.52	50.54	21.61	4.20	-	-	1	1	4.08
EI-085	2:1 RCO/LCO	0.70	3.96	2.65	3.89	9.05	63.78	8.02	7.96	-	-	3.4	3.6	7.56
EI-088	2:1 RCO/LCO	0.76	0.29	3.10	4.42	40.02	42.5	0.11	8.81	-	-	38.6	1000	15.67
EI-091	2:1 RCO/LCO	1.22	2.77	3.44	4.61	20.42	52.11	8.31	7.11	-	-	101	18.6	9.64
EI-094	2:1 RCO/LCO	0.99	5.06	2.89	3.29	9.00	58.64	13.16	6.98	-	-	3.4	9	6.28
EI-097	3:1 RCO/LCO	0.49	3.14	1.43	3.07	10.36	64.86	7.01	9.63	-	-	18.5	18.2	10.52
EI-100	3:1 RCO/LCO	0.84	0.69	1.17	4.53	27.32	54.86	1.91	8.68	-	-	9	162	11.26
EI-103	3:1 RCO/LCO	0.79	0.33	1.71	5.69	42.23	39.84	0.15	9.27	-	-	1100	64	33.62

MORPHOLOGY OF CARBON DEPOSITS AS A FUNCTION OF COAL-DERIVED JET FUEL CHEMICAL COMPOSITION

Ömer Gül, Leslie R. Rudnick, Harold H. Schobert

The Energy Institute,
The Pennsylvania State University,
University Park, Pennsylvania 16802

Introduction

Because of high thermal loads in future advanced aircraft, jet fuel will be exposed to much higher temperatures, reaching as high as 540°C, before combustion (1-3). At such high temperatures, both homogenous and heterogeneous reactions of jet fuel can lead to solid deposition on metal surfaces (4,5). The formation of carbonaceous deposits on metal surfaces in the fuel system is, therefore, a major concern for the development of advanced aircraft. Thermal stability of aviation jet fuel refers to its resistance to decomposition at elevated temperatures to form deleterious solid deposits.

Solid deposits from fuel degradation can attach to the surface of the flow lines or plug filters and create problems with the fuel system operation. The carbonaceous deposit formation appears to depend on a combination of different conditions, such as the reactivity of the starting fuel, the temperature, the pressure, the concentration, and the nature of the substrate surface.

Temperature is one of the most important parameters that affect the rate and reaction mechanisms of fuel degradation. Autooxidation of fuels takes place at temperatures less than 260°C, decomposition of oxygenated products at intermediate temperatures between 290 and 350°C, and pyrolysis at temperature greater than 350°C(6).

The composition of jet fuels is very complex. Many studies have been carried out with light hydrocarbons (7-11) to understand the mechanism of carbon formation on metals. One distinguishing property of carbon deposits is their oxidation reactivity, which depends on the chemical composition and the structure of the deposits. Differences in oxidation reactivity of the deposits are manifested in the evolution of CO₂ peaks at different temperatures during temperature-programmed oxidation (TPO) experiments (12,13). The TPO analysis is, therefore, useful to help understand the role of the metal surface in carbon deposit formation.

McCarty et al.(14) used temperature-programmed surface reaction with hydrogen to characterize carbon deposits produced on an alumina-supported nickel methanation catalyst upon exposure to carbon monoxide at 277°C. Based on the relative reactivity of the deposits toward hydrogen, the deposited carbon species were classified as chemisorbed carbon atoms (α) evolving around 190°C, bulk nickel carbide, amorphous carbon (β) around 385°C, filamentous carbon at 600°C, encapsulating carbon at 690°C, and crystalline graphite platelets at temperatures above 800°C.

This study examines the morphology of carbon deposits of thermally stressed hydrotreated 1:1, 2:1 and 3:1 blends of refined chemical oil (RCO) and light cycle oil (LCO), and JP-8 on Inconel 718 surface at 470°C fuel temperature.

Experimental

Thermal Stressing Experiments. The fuels tested in the thermal stressing experiments on Inconel 718 are coal-based blends HDT-(1:1 vol) RCO/LCO), HDT-(2:1 vol)RCO/LCO), HDT-(3:1 vol)RCO/LCO), and petroleum-based JP-8. The composition of Inconel 718 alloy and experimental procedure has been reported (15). Throughout all reported experiments, the reactor outlet

temperature, wall temperature, fuel pressure, and liquid fuel flow rate were kept at 470°C, 500°C, 17 atm., and 4 mL/min, respectively. The stainless steel preheating section is 2 mm in i.d. (1/8-in. o.d.) and 61 cm in length. The fuel residence time in this preheating zone is 22 sec. at a liquid fuel flow rate of 4 mL/min. The fuel residence time in the reactor (4 mm. i.d., 0.25 in. o.d. and 31.75 cm length) is 59 sec. at the same fuel flow rate. At the end of the reaction period (5 h.), the foils were cooled under an argon flow in the reactor. The details about the flow reactor system can be found in elsewhere paper (16).

Materials. Inconel 718 was obtained from Goodfellow Metals Ltd (Cambridge, U.K.)

Jet fuels hydrotreated to different severity used in thermal stressing tests were obtained from PARC. To verify the reproducibility of the experimental results, duplicate experiments of jet fuel stressing were carried out with different jet fuel blends in the presence of Inconel 718. The results of duplicate experiments showed that the TPO profiles were reproducible with respect to individual peak positions and relative peak intensities. The total amount of deposit measured on several different jet fuel blends were reproducible ± 10 (wt)% of the deposit.

Instrumental Analysis. Chemical composition of jet fuels was determined by GC/MS analysis.

Carbon Deposit Analysis; The deposited foils were analyzed using a LECO RC-412 multiphase carbon analyzer to determine the total carbon content and TPO profiles of the deposits on the foils. The surface morphology of the deposits was examined with an ISI-DS130 dual-stage scanning electron microscope (SEM). To examine the morphology of the carbon deposits on the strips, 1 cm long pieces were cut from the center of the strip.

Results and Discussion

In this study, morphology of carbon deposits and chemical composition were correlated. Chemical compositions of jet fuel samples were determined with GC-MS.

JP-8 fuel consists mainly of long-chain paraffins, with lower concentrations of alkyl cyclohexanes, alkyl benzenes, and alkyl naphthalenes. The coal derived-fuels consist of mostly tetralin, naphthalene, decalin and their alkyl substitutes, with lower concentrations of paraffins, saturated cyclics, alkyl benzenes and indanes. No indene or its derivatives were observed.

Exposure of jet fuel to high temperatures in aircraft fuel lines triggers pyrolysis reactions which eventually lead to deposition of carbonaceous solids on metal surfaces. This is particularly important problem for advanced future aircraft which may expose fuel to very high temperatures.

The chemical compositions of jet fuels have been reported recently (15). All of the coal derived-blends contain 40% or higher amount of tetralins, and also contain tricyclic compounds in the changing amount from 4.20 to 9.63%. The amount of other grouped compounds were varied according to hydrotreating severity.

The substrate temperature is a significant parameter having a major influence not only on the rate, but also on the type of carbonaceous deposition (8,17,18). In this study, different kinds of solid carbon deposits were observed with different coal derived-blends regarding to their chemical composition on Inconel 718 under the same conditions.

TPO profiles show peaks as a function of temperature. The different peaks observed in these plots can be evaluated as different natures of deposits. Observations from the TPO and SEM images of the deposits were discussed below.

Figure 1 shows the TPO profiles of the carbon deposits from thermal stressing of HDT-(1:1)RCO/LCO at 470°C and 250 psig

for 5h. Each fuel gave different TPO profiles. The major peak for 1:1 blends were observed at ~400°C.

The 1:1 blends (low saturated cyclics (<1%), decalins (<1%), and higher amount of naphthalenes (>19%)) gave the dominant peak at 400°C and also gave relatively high carbon signal. These peaks can be attributed to amorphous carbon and fine filaments as shown by the SEM image of EI-073 (Figure 2). These blends also gave lower temperature peaks (~150°C) which probably represent hydrogen-rich chemisorbed carbonaceous substance (16). Reactive deposits burn off at the lower temperatures, while less reactive deposits burn off at higher temperatures.

On the other hand, jet fuel blends, containing less aromaticity as naphthalenes (<5%) and higher amounts of saturated compounds, gave higher temperature peaks with lower carbon signal, i.e., TPO of EI-079.

Chemical compositions of EI-073 and EI-076 were very similar to each other, but their TPO profiles and SEM images (Figure 2 and Figure 3) were very different. One can conclude that, this difference might be related to their sulfur and nitrogen contents.

High temperature peaks (600°C) in the TPO profiles indicate the presence of relatively low reactive carbon deposits. Highly ordered structures in the deposits, having pre-graphitic or graphitic order would reduce the oxidation reactivity compared to that amorphous carbon with no apparent structural order (16). No deposits of this type were observed with 1:1 blended jet fuels based on TPO profiles.

TPO profiles in Figure 1 were obtained from thermal stressing of HDT- (1:1 vol.) RCO/LCO blends. The blends each gave different TPO profiles which could imply that carbon was deposited at different rates and perhaps by a different mechanism under the same conditions.

HDT-(2:1 vol.) RCO/LCO blends gave broader bands than those of HDT-(1:1 vol.) RCO/LCO blends (Figure 4). TPO profiles of 2:1 blended fuels showed a similar trend but changing relative carbon signal, except EI-088. This can be concluded that they may undergo similar deposition mechanisms during thermal stressing of fuels as a result of their similar chemical compositions. EI-088 has the lowest saturated cyclics, decalins and tetralins among four 2:1 blends.

SEM image of EI-085 (Figure 5) shows that strip surface covered more orderly form than that of EI-088. SEM image of EI-088 has been given in Figure 6 and it shows that there was an agglomeration instead of covering the surface completely.

Figure 7 shows the TPO profiles of carbon deposits from thermal stressing of HDT-(3:1 vol.) RCO/LCO and JP-8 at 470°C and 250 psig for 5h. The chemical compositions of these blends (3:1) change, i.e., while the amount of saturated cyclics, decalins, tetralins decrease from EI-097 to EI-103, the amount of indanes, naphthalenes increased. Carbon deposition TPO profiles showed some change as a result of the chemical composition. For example, the peak intensity at ~150°C increased from EI-097 to EI-103. This could imply that increasing aromaticity and decreasing saturated compounds in fuels could result in more chemisorbed and more amorphous carbon formed on Inconel 718.

The SEM image of EI-088 showed agglomerated carbon deposits, whereas EI-103 showed deposits of a more uniform structure, evenly spread over the surface of the Inconel 718. Chemical compositions of these two fuels were similar, i.e., naphthalenes (~40%), tetralins (~40%), decalins (~0.11%), saturated cyclics (~0.30%). However the sulfur concentrations of EI-103 was significantly higher than for EI-088. Sulfur has been previously implicated with carbon deposition mechanism (19). This

difference could be the reason for that deposition and surface covering with different mechanism.

It was also seen from the SEM images of EI-097 and EI-100 that deposits obtained from these fuels has covered the surface completely.

TPO of JP-8 shows a major peak at 500°C and a minor peak at 150°C. These peaks could be attributed as pre-graphitic and chemisorbed peaks, respectively. It was seen from the SEM image of JP-8 that there was filamentous-like deposit and that the surface of metal coupon was almost fully covered with carbonaceous materials.

Conclusion

In this work it was seen that increasing the RCO/LCO ratio in the blend changed the deposit nature and increased the surface coverage. It was also observed that if two fuels having similar chemical compositions but different sulfur and nitrogen concentrations, the carbon deposit morphology or coverage was different.

Acknowledgement. Financial support for this work was provided by the U.S. Air Force Office of Scientific Research.

References

- (1) Edwards, T.; Zabarnick, S. *Ind. Eng. Chem. Res.* **1993**, 32, 3117.
- (2) Heneghan, S.P.; Martel, C.R.; Williams, T.F.; Ballal, D.R. *Trans. ASME J. Eng. Gas Turb. Power.* **1993**, 115, 480.
- (3) Hazlett, R.N.; Kirklin, P.W.; Daiv, P., Eds.; ASTM STP 1138; ASTM:Philadelphia, PA, **1992**.
- (4) Heneghan, S.P.; Zabarnick, S.; Ballal, D.R.; Harrison III, W.E. *Trans. ASME J. Eng. Gas Turbines Power.* **1996**, 118, 170.
- (5) Jone, E.G.; Balster, W.J. *Energy Fuels.* **1995**, 9, 610.
- (6) Song, C.; Eser, S.; Schobert, H.H.; Hatcher, P.G. *Energy Fuels.* **1993**, 7(2), 234.
- (7) Trimm, L.D. *Catal. Rev.-Sci. Eng.* **1977**, 16, 155.
- (8) Trimm D.L.; Albright, L.F.; Crynes, B.L., Corcoran, W.H., Eds.; Academic Press: New York, **1983**.
- (9) Baker, R.T.K.; Harris, P.S.; Walker P.L., Jr., Thrower, P.A., Eds.; Marcel Dekker Inc.: New York, **1978**.
- (10) Albright, L.F.; Tsai, C.-H.T.; Albright, L.F., Crynes, B.L., Corcoran, W.H., Eds.; Academic Press: New York, **1983**.
- (11) Froment, G.F. *Rev. Chem. Eng.* **1990**, 16(4), 293.
- (12) McCarty, J.G.; Wise, H. J. *Catal.* **1979**, 57, 406.
- (13) Marecot, P.; Akhachane, A.; Micheaud, C.; Barbier, J. *Appl. Catal. A: Gen.* **1998**, 169, 189.
- (14) McCarty, J.G.; Hou, P.Y.; Sheridan, D.; Wise, H.; Albright, L.F., Baker, R.T.K., Eds.; ACS Symposium Series 202; American Chemical Society: Washington D.C., **1982**; Chapter 13, p 253.
- (15) Rudnick, L. R.; Gül, Ö.; Schobert, H. H. ,Prepr. Pap.- Am. Chem. Soc., Div. Fuel Chem., **2004**, Phila., to be presented.
- (16) Altin, O.; Eser, S., *Ind. Eng. Chem. Res.* **2001**, 40, 596.
- (17) Albright, L.F.; Marek, J.C. *Ind. Eng. Chem. Res.* **1988**, 27, 755.
- (18) Baker, R.T.K.; Yates, D.J.C.; Dumenic, J.A.; Albright, L.F., Baker, R.T.K., Eds.; ACS Symposium Series 202; American Chemical Society: Washington, D.C., **1983**; Chapter 1, pp 1-22.
- (19) Altin, O.; Bock, G.; Eser, S. *Prepr. Pap.- Am. Chem. Soc., Div. Petroleum Chem.*, **2002**, 47(3), 208

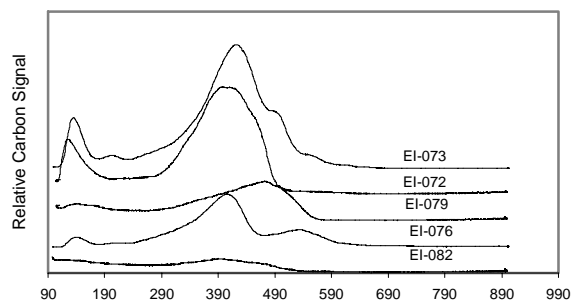


Figure 1. TPO profiles of carbon deposits from thermal stressing of 1:1 coal derived-jet fuels on Inconel 718

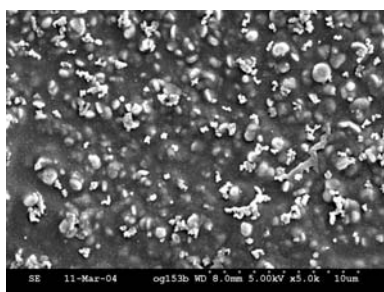


Figure 2. SEM image of carbon deposit from EI-073 at 470°C

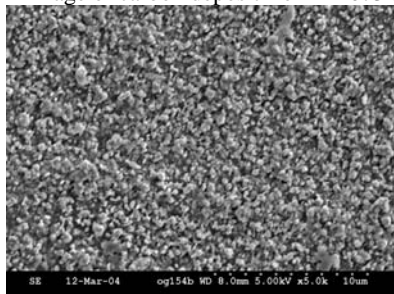


Figure 3. SEM image of carbon deposit from EI-076 at 470°C

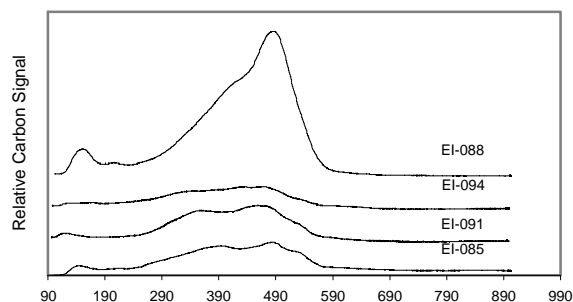


Figure 4. TPO profiles of carbon deposits from thermal stressing of 2:1 coal derived-jet fuels on Inconel 718 at 470°C

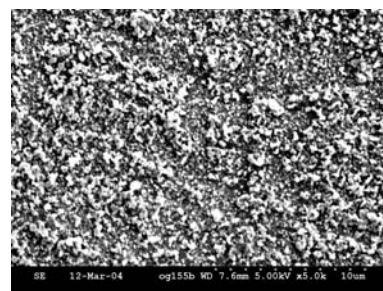


Figure 5. SEM image of carbon deposit from EI-085 at 470°C

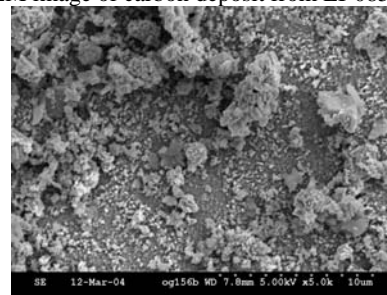


Figure 6. SEM image of carbon deposit from EI-088 at 470°C

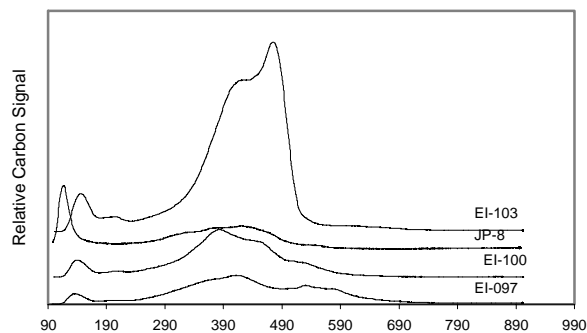


Figure 7. TPO profiles of carbon deposits from thermal stressing of 3:1 coal derived-jet fuels on Inconel 718 at 470°C

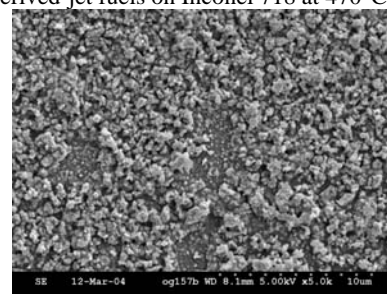


Figure 8. SEM image of carbon deposit from EI-103 at 470°C

FUTURE COILS FOR ETHYLENE FURNACES: REDUCED OR NO COKING AND INCREASED COIL LONGEVITY

Marvin G. McKimpton^a and Lyle F. Albright^b

^aInstitute of Materials Processing
Michigan Technological Institute
Houghton, MI 49931-1295

^bSchool of Chemical Engineering
Purdue University
West Lafayette, IN 47907-2100

Introduction

Significant improvements have occurred in reducing undesired coke production in ethylene furnaces and in increased longevity of the coils during the last 40 years and especially in the recent past. Filamentous coke which is catalyzed with nickel or iron is an excellent collection site for the coke formed by two distinctly different mechanisms (1). Inner surfaces of coils used in ethylene furnaces that are essentially free of nickel and iron do not produce these filaments. Baker and Chludzinski (2) have found that certain surfaces result in much lower levels of coke formation. Albright and Marek (3) found that the surface of metal had a large effect on the morphology of the coke; three distinct coking mechanisms produce coke deposits of very different character. The ability to collect coke or coke precursors is obviously an important factor relative to the amount of coke that eventually collects.

Coated Coils

In the last 5-10 years, several companies have publicized coils with inner surfaces that result in much reduced levels of coke formation. The following companies claim reduced coke deposits by factors of perhaps two to three: Alon Surface Technologies, Inc.; Westaim Surface Engineering Products; and Daido Steel (in cooperation with Royal Dutch/Shell Group). In all cases, rather thin coatings have been formed on the inner surfaces of high-alloy steels. These coatings have low concentrations of nickel, iron, and other metals that produce filamentous coke. It must be emphasized that at the high temperatures experienced in the coils that considerable diffusion of metal atoms occur in the walls of the coils and metal oxides form in the inner surfaces (4). In regular (non-coated) coils of high-alloy steels, the inner surfaces often become much enriched in oxides of chromium, manganese, aluminum, silicon, and titanium. Simultaneously, a sublayer enriched in iron and nickel forms. Claims have been made for these coils that the coatings are regenerated as the coil is used and as metal (or metal oxides, sulfides or carbides) are lost from the surface.

Additives

For many years, numerous additives have been mixed in relatively small amounts with the feedstocks to ethylene furnaces to reduce coke formation. Apparently in all cases, the additive changes the composition of the inner surfaces of the coil.

Compounds containing sulfur are widely used when ethane and propane are feedstocks. When naphthas and gas oils are feedstock, such additives are generally not needed since the feedstocks already contain adequate sulfur. Additives employed include hydrogen sulfide, dimethyl sulfide, dimethyl disulfide, mercaptans, etc. Although details are not known, these compounds decompose at the high temperatures releasing elemental sulfur. This sulfur plus other sulfur-containing intermediates react in part at least converting metal oxides on the surface to metal sulfides (5). Tests have shown that

hydrogen sulfide treatment of a coil that had just been decoked reduces coke formation immediately following decoking (6).

The following questions relative to sulfur compounds apparently have not been answered. (1) Which portions of the coil should be sulfided? Presumably the exit portion of the coil should be since here coking is most pronounced. (2) Can the method of introducing the compound be improved? In current methods, most sulfur is possibly freed and reacted before it reaches the exit end. Sulfide formation often contributes to reduced coil life.

Other additives have been reported, but explanations for the improvements are still needed. Several additives include:

- 1) Tin-silicon additive marketed by Chevron-Phillips. Presumably the surface of the coil is enriched with tin and silicon (probably as oxides).
- 2) An organo-phosphorus compound marketed by Nalco-Exxon is used in numerous furnaces plus at least two transferline exchangers (TLE's).
- 3) Technip Benelux have suggested a pretreatment that produces a silica layer on top of sulfur-treated metallic sublayer. Further dimethyldisulfide is continuously added.
- 4) SK Corp. provides an additive that forms an inner film containing silicon, chromium, and aluminum oxides plus alkali or alkali-earth metals. Alkali and alkali-earth metals have been reported to act as catalysts to promote the oxidation of coke (via carbon-steam reactions at high temperature).

A key question with all additives is can improved methods be developed to introduce the additive to the coil? The answer likely is yes.

Pretreated Coils

Nova Chemical Co. (7, 8) has reported that their pretreated coils often experience coke reductions by factors of 14-16 times. In one case, the time before decoking of a furnace using ethane-propane feedstock was extended to 520 days. One patent claims that chromium-manganese spinels are produced on the inner surfaces. Similar pretreatments were earlier investigated (9) and the data since analyzed (10). The stainless steels were pretreated with hydrogen-steam mixtures at 800-1000°C for extended periods of time. Nova's preferred conditions overlap those reported earlier.

The question, as yet unanswered, is why has coke formation been so greatly reduced as compared to other technologies just discussed. Two possible explanations are as follows: First, the coke and/or coke precursors fail to adhere to the pretreated surface. Examples were found earlier (9) of poor adherence. Second the pretreated surface act as a catalyst to promote gasification of the coke.

Longevity of Coils

The longevity of ethylene furnace coils is influenced by numerous factors, including furnace operating conditions, decoking practices and alloy selection. In many cases, coil service life is limited by carburization and localized tube wall thinning. Frequent and/or aggressive decoking practices appear to accelerate this carburization. An improved understanding of the inter-relationships between carburization and decoking is likely to be very useful for further extending coil life.

Alloy composition also has a substantial influence on coking characteristics and the coil longevity. Ethylene furnaces present some of the most severe operating conditions encountered anywhere in the chemical process industries. Coil materials experience coking, carburization, oxidation, creep and thermal cycling during service, and must be able to be welded for field installation. Over the last several decades, furnace temperatures have tended to rise, placing increasingly-stringent requirements on these coils.

Increasing coil longevity will require materials increasingly resistant to all of these phenomena but still exhibiting adequate fabricability. Most current coils are cast, fully austenitic modified HP alloys containing nominally 25 Cr and 35 Ni with “micro-alloying” additions of elements such as Nb, W, Ti, and Mo. This family of austenitic alloys, however, may be approaching its useful operating limits. Alloys with increased Cr and Ni contents show limited improvements in creep resistance and decreased melting points. Equally important, these alloys rely primarily on Cr coupled with low levels of Mn and Si to provide oxidation and carburization resistance. At higher temperatures, both increased rates of coking and the volatility of chromium oxides become a major concern.

Several groups, including Oak Ridge National Laboratory and Special Metals Corporation, are exploring alloys with higher aluminum contents. These materials have potential for higher melting temperatures, improved oxidation resistance, improved carburization resistance and reduced coking compared to current alloys. Ferritic oxide dispersion strengthened alloys such as Special Metal’s Incoloy[®] MA956 (Fe-20Cr-4.5 Al-0.5Ti-0.5Y₂O₃) also exhibit substantially higher creep resistance (11). Novel approaches such as clad tubes with a ferritic core and austenitic sheath are being considered to address concerns about material ductility and weldability. The current status of this work will be reviewed.

References

- (1) Albright, L.F.; Marek, J.C., *Ind. Eng. Chem. Res.*, **1988**, *27*, 755.
- (2) Baker, R.T.K.; Chludzinski, J.J., *J. Catalysis*, **1980**, *64*, 464.
- (3) Albright, L.F.; Marek, J.C., *Ind. Eng. Chem. Research*, **1988**, *27*, 751.
- (4) Luan, T.C.; Eckert, R.E.; Albright, L.F., *Ind. Eng. Chem. Research* **2003**, *42*, 4741.
- (5) Tsai, C.H.; Albright, L.F., *Industrial and Laboratory Pyrolysis*, ACS Symposium Series 32, L.F. Albright and B.L. Crynes, Eds., pp. 274-295, Amer. Chem. Soc., Washington, D.C., 1976.
- (6) Crynes, B.L.; Albright, L.F.; *Ind. Eng. Chem. Processes Design Develop.* **1969**, *8*, 25.
- (7) Benum, L., Achieving Longer Furnace Runs at Nova Chemicals, Spring Meeting, AIChE, New Orleans, 2002.
- (8) Benum, L.C.; Oballa, M.C.; Petrone, S.S.A.; Chao, W., Canadian Patent Applic. 2, 355, 436, March 27, 2002.
- (9) Szechy, G.; Luan, T.C.; Albright, L.F., Novel Production Methods for Ethylene, L.F. Albright and B.L. Crynes, Eds., Chapt. 18, Marcel Dekker, Inc., New York, 1992.
- (10) Luan, T.C.; Eckert, R.E.; Albright, L.F., *Ind. Eng. Chem. Research* **2003**, *42*, 4741.
- (11) Hosoya, K., et. al., Application of New Ethylene Furnace Tube—OxideDispersion Strengthened (ODS) Alloy, 13th Ethylene Forum, Baton Rouge, LA, 2001.

Ti AND Al OXIDE COATINGS ON INCONEL 718 AGAINST METAL SULFIDE FORMATION AND CARBON DEPOSITION FROM HEATED JP-8 FUEL

Orhan Altin^a, Semih Eser^a, Ajit R. James^b, and Xiaoxing Xi^b

^aThe Energy Institute

^bDepartment of Physics, 303 Davey Laboratory
The Pennsylvania State University
University Park, PA, 16802

Introduction

The trend of advanced aircraft toward increasing performance results in higher thermal loads and higher fuel temperatures and eventually the formation of carbon deposits on metal cooling line surfaces (1). The buildup of deposits in aircraft fuel systems is a major concern because it may lead to fuel system failure. Exposure of metal surfaces to jet fuel at temperatures higher than 400°C leads to the accumulation of carbonaceous deposits (2,3). Previous experimental results clearly showed that certain elements such as Ni, Co, Fe, and Mo in the fuel system dramatically increase fuel coking by catalyzing carbon deposit formation. On the contrary, the elements Ti, Al, Si, Cr, Ta, and Nb do not show much chemical, or catalytic activity upon heating with jet fuels to 500°C.

Thus, two inert surface coatings, Ti and Al oxides, were evaluated to investigate the potential for carbon deposit reduction. Among others, Marteny and Spadacini (4) suggested that two basic carbonaceous deposit formation processes occur: 1) A homogeneous oxidation reaction occurring in the fuel feedstream forming carbon particles which adhere to the fuel passage surface, 2) A heterogeneous catalytic reaction occurring at the fuel passage surface. Particularly for thermal stressing of jet fuels above 400°C, Mechanism 2 dominates leading to surface catalytic reaction between the reactive alloy elements and carbon deposit precursors. In addition to carbon deposit formation, sulfur compounds present in the fuel may react with transition metal elements on the alloy surfaces.

The effect of the trace amount of some sulfur compounds appears to be significant on the rate of deposit formation and metal surface degradation. The sulfidation of metals at high temperatures has become a matter of increasing concern in industrial applications, particularly in energy conversion systems using fossil fuel systems. Because of the high diffusivity and formation of eutectic melts with metals, sulfur reacts with metals at relatively low temperatures forming severe localized corrosion on heat-resistant alloys and superalloys (5-7).

Protective coatings on metal alloy surfaces may prevent contact between reactive fuel species and active metal surfaces to inhibit surface reactions and carbon deposition through heterogeneous reactions. Pulsed laser deposition is a relatively new method for the production of thin films. PLD provides a mechanism to deposit highly adherent thin films of a variety of tribological (friction, lubrication and wear properties) coatings. Donley and Zabinski (8) suggested that PLD films often exhibit superior performance as compared to those obtained by conventional coating techniques. Also, PLD offers the possibility of tailoring film properties by the appropriate choice of substrate materials, deposition parameters and after deposition treatments (9-10).

The objectives of this study were to coat Inconel 718 coupons with titanium and aluminum oxides by Pulse Laser Deposition and to investigate the effectiveness of these coatings in inhibiting carbon deposition and metal sulfide formation from heated JP-8 fuel.

Experimental

Mechanically polished Inconel 718 coupons were coated with Ti and Al oxides using Pulsed Laser Deposition (PLD). An eximer laser (Lambda Physik, LEXTRA 300C) was used as energy source to provide KrF laser irradiation (wavelength= 248 nm, pulse duration= 34ns) which was focused by a silica lens on the target through a quartz window. The laser at a repetition rate of 5Hz was applied for 10 min on the TiO₂ target (i.e., 5x10x60 = 3000 shots were used) and for Al₂O₃, 10 Hz was applied for 15 min., (i.e. 10x15x60 = 9000 shots). The high purity O₂ (99.995%) was introduced into the chamber through a fine control valve. The substrate temperature was kept at 500°C throughout the coating processes. The oxygen pressure was 10⁻⁴ torr. Prior to coating, the Inconel 718 substrate surfaces were ground by using 320, 600, and 1200 grade SiC abrasive disks and polished by 0.5μ diamond suspension on red felt.

Thermal stressing Experiments. The thermal stressing of JP-8 fuel in the presence of Ti and Al oxides coated Inconel 718 superalloy foil (Goodfellow Co.) was performed in 1/4" (OD) glass-lined flow-through reactor. The elemental composition of Inconel 718 (wt %) is as follows: Ni:52.5, Fe:18.5, Cr:19, Mo:3.05, Al:0.5, Ti:0.9, Nb+Ta:5.13, Cu:0.15, Mn:0.18, Si:0.18, C:0.04, S:0.0008. The foils, 15x0.3 cm, were placed at the bottom of 20 cm long reactor. The reactor was preheated to 515°C for 2 hours in flowing argon at 34 atm before introducing the fuel. The fuel was preheated to 250°C in a valve oven before entering the reactor. The fuel flow rate was kept at 4mL/min.

The morphology of the substrate, Ti and Al oxide deposited films, and carbon deposits was examined by using field emission scanning electron microscopy (FESEM, JEOL JSM-6300F), transmission electron microscopy (TEM, Philips EM420ST) scanning electron microscopy (Hitachi S-3400N), and tapping mode atomic force microscope (AFM, Digital Instruments- Dimension 3100). The structure of the thin films was examined by glancing incidence X-ray diffraction (XRD, Philips) where incident angle was fixed at a value of 1°.

Results and Discussion

Surface morphology and structure characterization. The thickness of the TiO₂ and Al₂O₃ coatings obtained on alloy substrates was approximately 1 μm. FESEM images showed that the polished Inconel 718 surface prior to coating is very smooth. The SEM images showed that the smooth substrate surface resulted in the formation of smooth coatings through uniform nucleation of the precursor and smooth growth of the oxide crystals. It was observed that polycrystalline morphology of the Ti oxide coating on Inconel 718 with average crystallite diameter of 0.2 μ. In contrast, Al oxide coating appears to be featureless. The thickness of Ti and Al oxide coatings was 1.1 μm and 1.0μm, respectively, as measured by SEM cross-section examination.

Tapping mode AFM topographic images in Figure 1 show that coatings of Ti and Al oxides on polished Inconel 718 surface are quite smooth because of the smooth substrate surface. While the average roughness value of Inconel 718 is approximately 10 nm, the coated surface roughness values for Ti and Al are 23.7 and 12.9 nm, respectively.

Grazing Incident X-ray diffraction analysis was applied for the identification of TiO₂ and Al₂O₃ thin film phases deposited on Inconel 718 surfaces. The angle between the incident X-ray and coated surface was 1°. GIXRD patterns showed that the TiO₂ deposition was in the form of anatase and Al oxides were mostly in the amorphous form on Inconel 718 surface after 10 min PLD deposition. The TiO₂ coating on Inconel 718 surface produced mainly anatase phases without leading any outward cation diffusion

from the substrate. Since the substrate temperature was 500°C, anatase, rather than brookite, or rutile, formed. GIXRD results indicate that at 500°C substrate temperature, the crystalline Al oxide phase does not form. Stable Θ -Al₂O₃ and α -Al₂O₃ phases form at 900-1000°C and 1000-1100°C in oxygen atmosphere. Hirschauer et al. (11) studied different substrate temperatures to obtain crystalline α -Al₂O₃ on Si (111) wafers by using PLD and obtained highly crystalline α -Al₂O₃ structures at 850°C substrate temperature. They reported that below 850°C metallic Al was observed because of the higher desorption rate of oxygen than aluminum from the surface. However, for our case higher substrate temperature would result in creation of oxide layers which will affect the coating mechanism and adhesion. At 500°C substrate temperature surface diffusion length is smaller than the adsorbed species diameter, Ti and Al, which did not lead to significant void or dome formations.

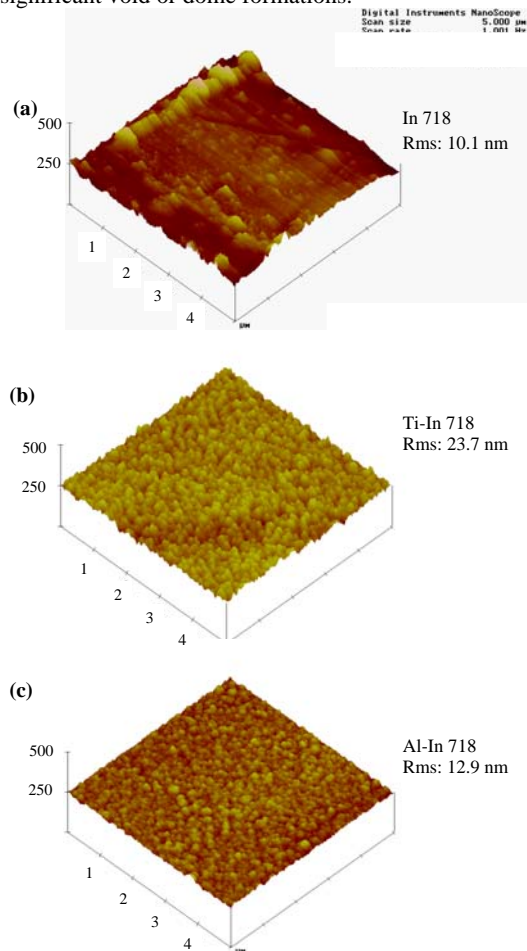


Figure 1. AFM images of polished Inconel 718 substrate (a), Ti oxide coated (b), and Al oxide coated (c) Inconel 718 surfaces.

Thermal Stressing of JP-8 Fuel on Alloy Substrate and Coated Surfaces. The JP-8 thermal stressing experiments were carried out on both bare substrate and Ti and Al oxides coated Inconel 718 surfaces at 470°C fuel temperature and 34 atm for 24h with a 4 mL/min flow rate.

Bare Inconel 718 substrate surface collected significant amount of carbon and sulfur deposits from JP-8 decomposition at 470°C and 34 atm after 24h as shown in Figure 2. Figure 2 shows SEM and TEM images of the stressed Inconel 718 surface indicating the presence of faceted crystalline metal sulfides, carbon filaments and

amorphous carbon structures. The X-ray diffraction and EDS analysis results indicated that the metal sulfides consist of Ni₃S₂, Ni_{1-x}S, and Fe_{1-x}S. These observations show that the bare Inconel 718 surface was significantly corroded by the formation of sulfide crystallites that are approximately 0.5 μ m or smaller in diameter. As seen in Figure 2a, the formation of sulfides reconstructs the metal surfaces to produce very fine faceted structures which are especially important in catalytic reactions that lead to structured carbon deposits.

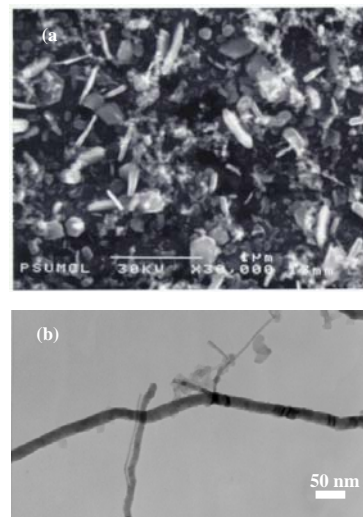


Figure 2. SEM (a) and TEM (b) images of carbon and sulfur deposits from JP-8 decomposition at 470°C fuel temperature and 34 atm for 24h on bare Inconel 718 surface.

Figure 2b shows a TEM image of filamentous carbon and nanotubes produced on Inconel 718 at 470°C fuel temperature. The filaments are 10 to 15 nm in diameter and 2-5 μ m in length. The micrograph also shows carbon nanotubes (4-6 nm in diameter) as well as spherical carbon deposits growing on the surface of the filaments containing metal particles which are presumably Ni and Fe. Thermal decomposition of jet fuels produces reactive gas species which are chemisorbed on metal surfaces. The Ni, Co, and Fe rich alloy surfaces catalyze decomposition of chemisorbed hydrocarbons to produce carbon and hydrogen. Carbon then diffuses through any dislocations on the metal surface and finally precipitates in these locations as solid deposit (12,13). The increased concentration of precipitated carbon creates a stress at dislocations, and after a certain tensile strength of the metal is reached, the metal crystallite is removed from the surface producing a filament with a metal particle at the tip.

From our baseline experiments, and previous work in this laboratory, it becomes clear that the chemical composition of metal alloy surfaces, in particular, the activity for producing filamentous carbon plays a critical role in initiating the deposition process. Roughness of the substrate surface could also play an important role for the accessibility of the active sites and the chemisorption of deposit precursors.

The coated substrates were stressed with JP-8 under the same conditions that the bare Inconel 718 was stressed (at 470°C for 24 h.), and the stressed samples were examined by FESEM/EDS. As shown in Figure 3, both coatings appeared to be effective in inhibiting the catalytic activity of the bare metal surfaces. On both Ti and Al oxide surfaces, the deposit amount was significantly low compared to bare substrate surface because of the higher thermodynamic stability of TiO₂ and Al₂O₃ films. Lesser degree of

carbon deposit formation was observed on Ti oxide coated surface than on Al oxide coated surface. The morphology of deposits is almost similar for both coated surfaces. They consist of apparently amorphous solids. Thus, Ti and Al oxide coatings appear to collect only amorphous deposit. No filamentous carbon was observed on the TiO₂ and Al₂O₃ coated surfaces.

The amount of carbon deposit on the TiO₂ coated surface is lower than that on the Al₂O₃ coated surface as seen in Figures 3a and 3b. Agglomerated amorphous deposits observed on the Al₂O₃ coated surfaces (Figure 3b) can be attributed to the presence of some metallic Al on the surface that tends to react with sulfur and carbon. It is well known that aluminum plays a significant role as an alloying addition, determining the scaling resistance of materials in oxygen, sulfur and carbon containing environments. Addition of aluminum content of about 5% in the alloys based on Fe-Cr, Co-Cr, and Ni-Cr greatly improve the sulfur corrosion resistance of the alloy if good protective α -Al₂O₃ scale formed.

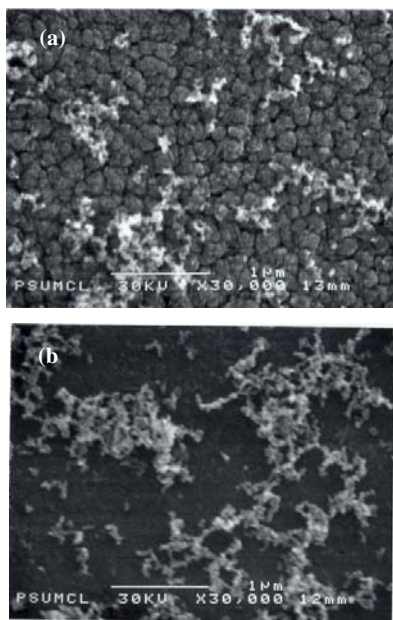


Figure 3. FESEM images of carbon deposits from JP-8 decomposition on Ti (a) and Al (b) oxide coated Inconel 718 surface at 470°C fuel temperature and 34 atm for 24h at a 4 mL/min flow rate.

Conclusions

Approximately 1 μ m coatings of Al and Ti oxides were obtained on Inconel 718 coupons using pulsed laser deposition. JP-8 fuel stressing at 470°C and 34 atm in the presence of bare and coated Inconel 718 coupons indicated that both coatings reduced carbon deposition by eliminating the catalytic activity of the metal alloy surface. In addition, no metal sulfide formation was observed on the Ti and Al oxide coated surfaces after thermal stressing with the JP-8 fuel. The Al oxide coated surface collected a larger amount of carbon deposit than the Ti oxide coated surface presumably because of the presence of metallic Al in the former. For better and efficient coating of stable α -Al₂O₃ oxide, the substrate temperature can be increased to 850°C to reduce the metallic Al formation. This may totally eliminate sulfur corrosion and subsequent surface roughening upon stressing with the jet fuel.

Acknowledgement. This work is part of a project funded by the Air Force Office of Scientific Research.

References

- (1) Zabarnick, S.; Zelesnik, P.; and Grinstead, R. R. *J. Eng. Gas Turb. Pow.* **1996**, 118 271.
- (2) Maurice, L. Q.; Lander, H.; Edwards, T.; and Harrison III, W. E. *Fuel*, **2001**, 80, 747.
- (3) Diane, L. L.; Meyer, M. L.; Edwards, T.; and Eitman, D. A. *33rd Joint Propulsion Conference and Exhibit*, AIAA-97-3041, Seattle, Washington, July 6-9, 1997.
- (4) Marteney, P. J.; and Spadicini, L. J., *ASME Paper* 91-GT-36, June 1991
- (5) Altin, O.; and Eser, S., *Ind. Eng. Chem. Res.* **2001**, 40 589.
- (6) Altin, O.; and Eser, S., *Ind. Eng. Chem. Res.*, **2001**, 40, 595.
- (7) Narita, T.; and Ishikawa, T., *Mat. Sci. Eng.* **1987**, 87, 51.
- (8) Donley, M. S.; and Zabinski, J. S., *Tribological Coatings, In Pulsed Laser Deposition of Thin Films*, D. B. Chrisey, G. H. Hubler (Eds.), Wiley, NY, Chp.18, 1997.
- (9) Sturm, K.; Fahler, S.; and Krebs, H.U., *Appl. Surf. Sci.*, **2000**, 154, 462.
- (10) Yin, X.; Miura, R.; Endou, A.; Gunji, I.; Yamauchi, R.; Kubo, M.; Stirling, A.; Fahmi, A.; and Miyamoto, A., *Appl. Surf. Sci.* **1997**, 119, 199.
- (11) Hirschauer, B.; Soderholm, S.; Chiaia, G.; and Karlsson, U. O., *Thin Solid Films*, **1997**, 305, 243.
- (12) Bianchini, E. C. ; and C. R. F. Lund, *J. Catal.*, **1989**, 117 455.
- (13) J. -W. Snoeck, G. F. Froment, and M. Fowles, *J. Catal.* 169 (1997) 240.

MODELING ELEMENTARY REACTIONS IN COKE FORMATION FROM FIRST PRINCIPLES

Veronique Van Speybroeck, Marie-Françoise Reyniers[#],
Guy B. Marin[#] and Michel Waroquier

Laboratory of Theoretical Physics, Center for Molecular Modeling,
Ghent University, Proeftuinstraat 86, B-9000 Gent, Belgium and
[#]Laboratorium voor Petrochemische Techniek, Universiteit Gent,
Krijgslaan 281-S5, B-9000 Gent, Belgium

Introduction

Thermal cracking of hydrocarbons is the simplest and oldest method for petroleum refinery processes and is considered as the main process for the production of light olefins such as ethene. The thermal cracking of hydrocarbons is known to proceed through a free radical chain mechanism. Radicals are mainly formed via C-C bond breaking and propagation occurs through abstraction and addition reactions. Decomposition of radicals by β -scission results in the desired gas-phase olefins. During this process, highly undesirable carbon-rich products are formed on the inner walls of the reactor giving rise to the formation of a coke layer. This coke layer has a negative influence on the efficiency of the cracking unit.

The process of coke formation is a complex phenomenon^{1,2}. Initially coke is formed by a heterogeneous catalytic mechanism in which the properties of the inner tube skin play an important role. Once the metal surface is covered with coke the catalytic activity of the metal particles diminishes and a heterogeneous non-catalytic mechanism becomes important. The coke layer thus formed has a polynuclear aromatic character. Usually one focuses on the second process since the period of catalytic coke formation is very small with respect to the total run length.

In today's operation of a plant simulation models play a very important role. Recently a coking model based on elementary reactions was developed at the Laboratorium voor Petrochemische Techniek^{3,4}. In view of the fundamental nature of the elementary steps considered such a model is of general applicability. One of the main challenges in the development of an accurate and broadly applicable model is the assignment of values for rate coefficients of the individual reactions occurring in the reaction network. The fundamental nature of the elementary steps considered allows the use of theoretical calculations to provide kinetic and thermodynamic data and to obtain microscopic insight in the basic reaction steps of the coke formation model. The elementary reaction steps that lead to incorporation of carbon atoms and growth of the coke surface can be divided in five classes of reversible reactions (cf. Fig. 1):

- (i) Hydrogen abstraction reactions by gas phase radicals and reverse reactions
- (ii) Substitution reactions by radicals at the coke surface and reverse reactions
- (iii) Addition reactions of radical surface species to gas phase olefins and the inverse β -scission of a radical surface species in smaller surface species and gas phase olefins
- (iv) Addition reactions of gas phase radicals to olefinic bonds in a surface species and the inverse decomposition of radical surface species to gas phase radicals and olefinic surface species
- (v) Cyclization of radical surface species and decyclization

Due to the increasing capabilities of computing power and optimization of numerical models it is now possible to perform high level ab initio calculations on systems of industrial importance. Kinetic parameters, such as the preexponential factor and activation energy, can be obtained by means of Transition State Theory (TST). The microscopic quantities are obtained by means of ab initio

calculations. In this work preference has been given to Density Functional Theory calculations, since this approach is computationally attractive for the larger structures that are involved in this work. This approach has been successfully applied to a variety of important chemical reactions.

In the first part of this paper, microscopic routes starting from benzene leading to the formation of naphthalene are investigated with the aim to identify important coke precursors and to obtain insight into the elementary reaction classes that determine the rate of coke formation. In the second part of the paper, larger polyaromatic clusters are considered in order to determine the influence of the coke matrix on the kinetics of the elementary reactions.

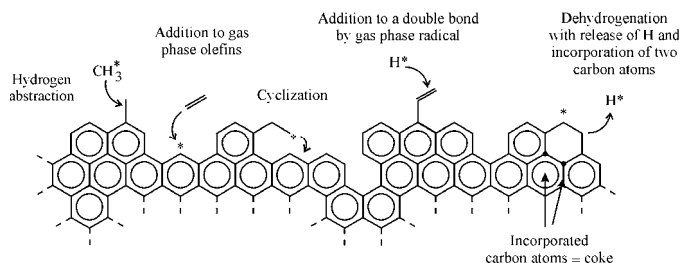


Figure 1. Radical elementary reaction steps leading to coke growth.

Microscopic pathways for the formation of naphthalene from benzene.

In order to obtain microscopic insight into the elementary reactions leading to cokes, various pathways are studied starting from benzene that lead to the formation of naphthalene. For this study the coke layer is approximated by only one benzene ring. The composition of the process gas is an important factor in the coke formation. A lot of work in this research field has been done by Kopinke et al., who performed tracer experiments with ¹⁴C-labeled hydrocarbons added to straight run naphtha to establish structure-reactivity relations and relative coking rates for various types of hydrocarbons⁵. The most important coke precursors were found to be olefins and aromatics. Ethene has the lowest coking tendency of the olefinic hydrocarbons but its high concentrations in the gas phase, explains its large contribution to the coke formation in a thermal cracking unit. Propene shows similar properties. Ethyne is more reactive than ethene but appears in much smaller concentrations, limiting its contribution to coke formation. To investigate these earlier experimental findings all reaction routes with ethyne and ethene as typical coke precursors are taken into consideration (cfr. Fig. 2).

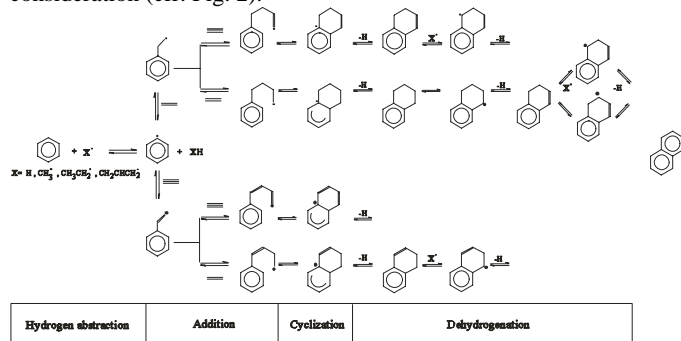


Figure 2. Radical elementary reaction steps leading to coke growth

The reaction sequence is initiated by hydrogen abstractions from benzene with gas phase radicals creating radical surface species. In turn these radicals react further with unsaturated gas phase components. Earlier experimental work indicated that hydrogen, methyl, ethyl and allyl radicals are very reactive in the coke

formation during thermal cracking⁶. Therefore all hydrogen abstractions in which the latter radicals are involved are taken into consideration. Based on the proposed reaction scheme, several conclusions concerning the coking tendency of gas phase components and the relative importance of the various reaction types can be drawn.

Influence of gas phase precursors on the coking rate. For all studied addition reactions with ethyne and ethene, both gas phase unsaturated components yield activation energies which are in the same order of magnitude, with respect to each other. The preexponential factor for reactions with ethyne is higher than for the corresponding additions with ethene, resulting in relative rate constants for additions to ethyne that are approximately twice as high as the ones for additions to ethene.

To estimate however the relative importance of both gas phase components as a coke precursor, their concentration has to be taken into account also. Gas phase concentration profiles were obtained from a simulation program, which is based on a detailed network of elementary reactions, developed at the Laboratorium voor Petrochemische Techniek^{7,8}. The reactor geometry and the operating conditions are taken for a typical ethane cracking unit. The process gas temperature profile as a function of the axial reactor coordinate is shown schematically shown in fig. 3 and varies between 800 K at the reactor inlet to reach a coil outlet temperature of 1100 K.

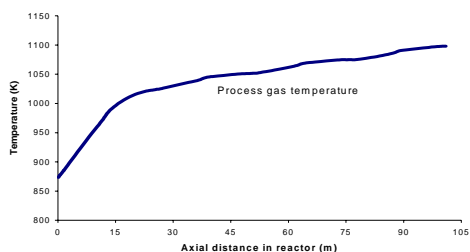


Figure 3. Temperature profile of the process gas along the reactor coil for typical ethane cracking conditions.

Typical concentrations of ethene and ethyne were obtained at the reactor inlet, in the middle of the reactor length and at the outlet the reactor. These values are presented in Table 1.

Table 1. Concentrations of ethyne and ethene at various axial reactor distances during ethane cracking.

Axial distance (m)	Ethene (mol/dm ³)	Ethyne (mol/dm ³)
1.09	$2.52 \cdot 10^{-7}$	$1.51 \cdot 10^{-15}$
44.02	$3.14 \cdot 10^{-3}$	$3.90 \cdot 10^{-6}$
100.96	$5.88 \cdot 10^{-3}$	$5.35 \cdot 10^{-5}$

Taking these concentrations into account, ethene shows the highest coking tendency despite its lower reaction rates. This result is in accordance with earlier reported experimental data⁵. However, at the higher temperatures prevailing in the last passes of the reactor, the coking tendency of ethyne becomes more important due to the smaller difference in concentrations between the two unsaturated hydrocarbons.

Relative importance to coke formation of the various reaction types. At second instance it is interesting to search for rate determining reaction steps along the reaction sequence going from

benzene to naphthalene. Since the reaction network contains both bimolecular and unimolecular reactions, it is not possible to compare directly the rate constants of the elementary reaction steps. Again concentration profiles have to be taken into account to compare absolute rates of the various reaction steps. It is found that the initial hydrogen abstraction are relatively slow, due to the low concentration of the gas phase radicals. The individual rate constants however were found to be one of the highest in the total reaction network. The initially created radical surface species can further grow by means of various subsequent additions. The first addition of ethene or ethyne to the phenyl radical is characterized by a high rate constant. This can be explained by the reactivity of the phenyl radical. The subsequent additions are much slower and determine the coking efficiency. After the second addition all further reaction steps, i.e. the cyclizations and dehydrogenation, proceed very fast. Previous discussion reveals that the initial creation of surface species and the subsequent additions determine the coking efficiency of the reaction network.

Influence of the coke matrix on the kinetic parameters

The reaction network discussed in the previous section was based on the assumption that the coke surface could be approximated by only one benzene ring. It is however important to investigate the validity of this approximation. Therefore calculations were performed on larger polyaromatic compounds to establish the importance of the local environment of the active surface site in the coke formation.

Classification of PAHs based on Bond Dissociation Energies.

A measure of the chemical reactivity of a site at an aromatic cluster is the bond dissociation energy (BDE) of the corresponding C-H bond. BDEs of all C-H bonds were calculated for the series of PAHs shown in fig. 4.

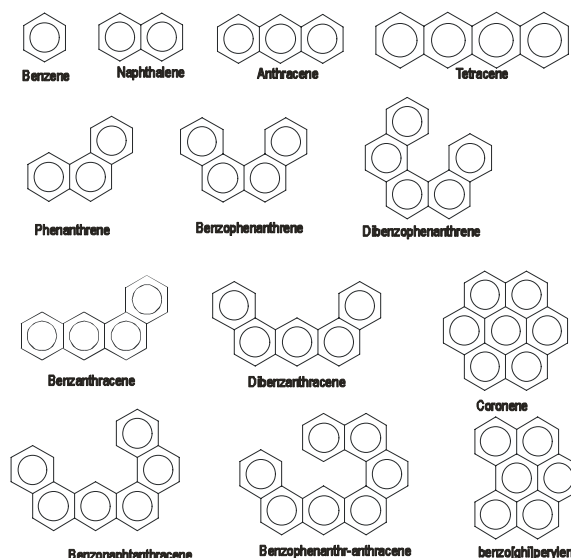


Figure 4. PAHs considered in this study

Based on the BDEs the C-H bonds in aromatic structures can be divided into four types with different reactivity, which can be related to the local structure around the site (Fig. 5). Similar conclusions were made by various other authors⁹.

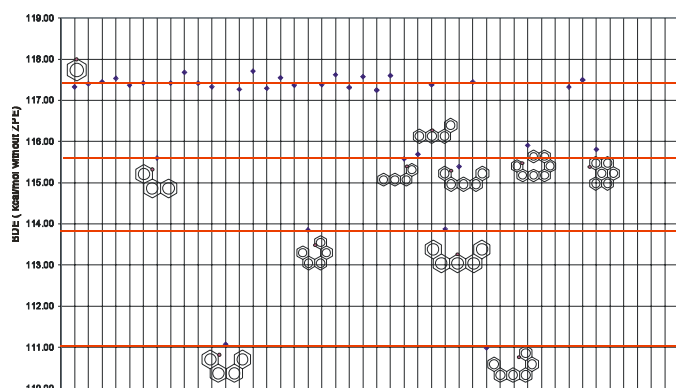


Figure 5. BDEs for a series of PAHs

The types of sites at the coke surface are defined based on their reactivity as well as on the structure of the local surroundings. Although benzene, naphthalene and anthracene have similar reactivities, they are retained as separate surface sites for further kinetic calculations due to their structural differences. This results in six different sites which are based on differences in local structure and/or on differences in chemical reactivity. The six different sites are named according to the smallest aromatic compound that exhibits the same local structure i.e. a benzene-like, naphthalene-like, anthracene-like, phenanthrene-like, benzophenanthrene-like and dibenzo(c,g)-phenanthrene-like site.

Kinetics of hydrogen abstraction reactions on PAHs.

Attention is focussed on the influence of the local polyaromatic structure on the kinetic parameters of hydrogen abstractions reactions with a methyl radical. The latter reactions are known to determine the global coking rate. The kinetic parameters are determined for six different sites as introduced in the previous section. A conformational and vibrational analysis was performed for each of the reactants, products and transition states at the B3LYP/6-311G** level of theory. The resulting kinetic parameters, calculated in the temperature interval from 700 to 1100 K which is characteristic for thermal cracking, are given in table 2.

Table 2. Kinetic parameters (700-1100K) for hydrogen abstractions at PAHs

Hydrogen abstraction	Ea (kJ/mol)	A (m ³ /mol.s)
at benzene-like site	79.68	1.7 10 ⁹
at naphthalene-like site	81.82	8.2 10 ⁷
at anthracene-like site	84.63	2.4 10 ⁸
at phenanthrene-like site	85.94	1.7 10 ⁷
at benzophenanthrene-like site	85.42	4.8 10 ⁶
at dibenzo(c,g)-phenanthrene-like site	85.81	4.5 10 ⁶

The microscopic calculations give insight into the factors that determine the kinetic parameters. The activation energy varies only slightly in terms of the local PAH structure. The small differences must be traced back to the steric hindrance between the attacking methyl radical and the polyaromatic structure. The frequency factor however varies largely with the number of aromatic rings involved in the polyaromatic structure. These variations must be traced back to the occurrence of skeletal vibrations in the larger PAH structures. For larger PAH structures more skeletal vibrations are present in the reactant structures and thus the PAH obtains a larger degree of

conformational flexibility and a larger partition function. This results in smaller rates for hydrogen abstractions at larger polyaromatics. This is further illustrated by comparing absolute rates in the temperature interval which is typically encountered in an industrial cracking unit. The relative rates for hydrogen abstractions with a methyl radical at site X (X= naphthalene, anthracene, phenanthrene, benzophenanthrene) with respect to a benzene-like site are presented in fig. 6.

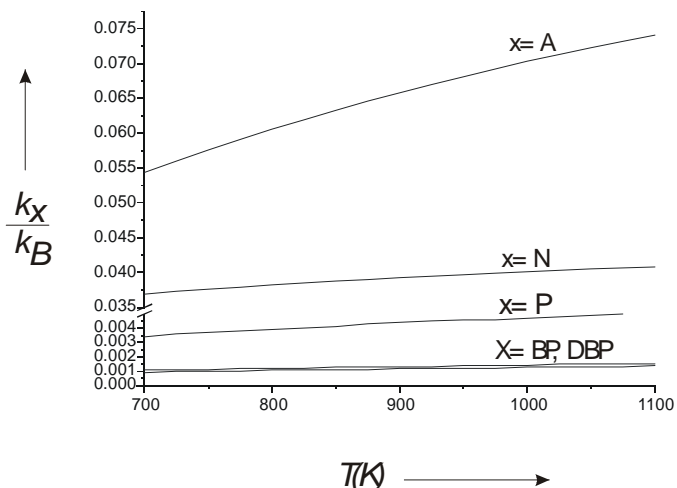


Figure 6. Rate constant for hydrogen abstractions with a methyl radical at site X, relative to the rate constant at the B site, as a function of temperature.

The initial creation of radical surface species predominantly occurs at the smaller clusters and preferentially at a benzene-like site. For other elementary classes of the coke formation network, also a strong correlation was observed between the size of the PAH and the rate constants^{10,11}.

Conclusions

In this paper, various elementary reaction steps important for coke formation during thermal cracking of hydrocarbons are studied. In a first instance all elementary reaction steps of a reaction network starting from benzene and leading to naphthalene were studied. The importance of various gas phase components as coke precursors was evaluated by considering all reaction routes in which ethene and ethyne are involved. It was shown that, despite its lower reactivity in the various elementary steps, ethene is an efficient coke precursor due to its high concentration. Although ethyne is more reactive, it contributes only significantly to coke formation at higher axial distances in the reactor. The theoretical calculations of the rate constants also reveal that the initial hydrogen abstractions and the subsequent addition occur at lower rates than cyclization and dehydrogenation reactions.

In a second instance, the kinetic calculations were extended to larger polyaromatics, to investigate the influence of the local environment of the coke surface on the kinetic parameters. A classification for the reactivity of PAH's based on BDE's was proposed. Four different classes of C-H bonds could be identified. Based on reactivity and local structural difference six types of active sites for coke growth were identified. The influence of the local environment of the active site on the kinetics was investigated by studying a series of hydrogen abstraction reactions. The latter reaction class was derived to determine the global coking rate of the reaction network. It was found that the rate constants can vary largely depending on the local structure of the polyaromatic surface.

Moreover at typical temperatures encountered during cracking, hydrogen abstractions preferentially occur at the smaller PAHs, such as benzene, naphthalene and anthracene.

Acknowledgement. This work is supported by the Fund for Scientific Research-Flanders (FWO) and the Research Board of Ghent University

References

- (1) Wauters,S; and Marin, G.B., *Ind.Eng.Chem.Res.*, **2002**, 41(10), 2379.
- (2) Wauters,S; and Marin, G.B. , *Chem.Eng.J.*, **2001**, 82(1-3), 267.
- (3) Wauters,S, PhD Thesis. *Kinetics of coke formation during thermal cracking of hydrocarbons based on elementary reactions*, **2001**, Ghent University
- (4) Van Geem,K.M.; Heynderickx, G.J.; Marin,G.B.; *AIChE Journal*, **2004**, 50, 173-183.
- (5) (a) Kopinke,F.D.; Zimmerman,G.; Nowak,S., *Carbon*, **1988**, 26(2), 117-124. (b) Kopinke,F.D.; Zimmerman,G.; Reyniers,G.C.; Froment, G.F., *Ind.Eng.Chem.Res.*, **1993**, 32, 56-61. (c) Kopinke,F.D.; Zimmerman, G.; Reyniers,G.C.; Froment, G.F., *Ind.Eng.Chem.Res.*, **1993**, 32, 2620-2625.
- (6) Froment, G.F. *Fouling of heat transfer surfaces by coke formation in petrochemical reactors*, in E. Summerscales, J.G. Knudson (Eds.), *Fouling of Heat Transfer Equipment*, Hemisphere Publ. Corp., **1981**.
- (7) Clymans, P.J.; Froment,G.F., *Comput.Chem.Eng.*, **1984**, 8, 137-142.
- (8) (a) Reyniers, G.C.; Froment,G.F.; Kopinke,F.D.; Zimmerman,G., *Ind. Eng.Chem.Res.*, **1994**, 33(11), 2584-2590. (b) Plehiers,P.M.; Reyniers,G.C.; Froment,G.F., *Ind. Eng.Chem.Res.*, **1990**, 29, 636-641.
- (9) (a) Aihara,J.; Fujiwara,K.; Harada,A.; Ichikawa,H.; Fukushima,K.; Hirota,F.; Ishida,T.; *J.Mol. Struct. (Theochem)*, **1996**, 366, 219-226. (b) Chen, R.H.; Kafafi,S.A.; Stein,S.E.; *J.Am.Chem.Soc.*, **1989**, 111, 1418-1423. (c) Cioslowski,J.; Liu,G.; Martinov,M.; Piskorz,P.; Moncrieff, D.; *J.Am.Chem.Soc.*, **1996**, 118, 5261-5264. (d) Stein,S.E.; Brown,R.L., *J.Am.Chem.Soc.*, **1991**, 113, 787-793. (e) Wang,H.; Frenklach,M.; *J.Phys.Chem.*, **1993**, 97, 3867-3874.
- (10) Van Speybroeck, V.; Reyniers,M.F.; Marin,G.B.; Waroquier, M.; *ChemPhysChem*,**2002**, 3, 863-870.
- (11) Van Speybroeck,V.; Hemelsoet,K.; Waroquier,M.; Marin,G.B.; *Int. J.Quant.Chem.*, **2004**, 96, 568-576.

AUTOMATED MODELING OF GAS-PHASE CHEMISTRY FOR PYROCARBON-FORMING HIGH-CONVERSION ETHANE PYROLYSIS

David M. Matheu^a, Jeffrey M. Grenda^b

^aNational Institute of Standards and Technology
Physical and Chemical Properties Division
100 Bureau Dr. Stop 8380
Gaithersburg, MD 20899-8380

^bExxonMobil Research and Engineering Company
1545 Rt. 22 East
Annandale, NJ, 08801

Introduction

Pyrolytic carbon deposition remains a key problem for the industrial cracking of light alkanes, and the deposition rate depends in part on the chemistry of the gas phase. The deposits degrade heat transfer efficiency, and must be periodically removed from pyrolysis reactors, necessitating expensive shutdowns. Furthermore, in the intentional deposition of pyrolytic carbon material from small hydrocarbons, the gas-phase chemistry has important effects on the quality of the carbon deposited [1]. But the processes leading to pyrolytic carbon deposition are still seriously debated in the literature.

Glasier and Pacey recently performed a series of neat ethane pyrolysis experiments focused on the gas-phase products and pyrocarbon deposition rates at very high conversion (900-1200 K, 0.4 atm, conversion > 98%) [2]. The large “soup” of species and reactions at such high conversion, however, makes developing an appropriate detailed chemical kinetic model extremely difficult; to our knowledge, no published model exists which is appropriate to the experimenters’ conditions. That is unfortunate, since a reliable model for the Glasier and Pacey experiments could be useful, as an intermediate step, toward the ultimate understanding of how the higher aromatic species are formed and deposited in pyrolysis systems.

In this work we apply a new, automated mechanism generation tool, called “XMG-PDep” [3;4], to rigorously construct an elementary-step-based chemical kinetic model for the conditions of the Glasier and Pacey experiments. We then apply reaction pathway analysis, sensitivity analysis, and equilibrium analysis to understand those chemical pathways that control the formation and destruction of the minor products measured by the experimenters. The results suggest that rarely considered pathways may play key roles in minor product chemistry, and proper, systematic treatment of the pressure-dependence is important for all the minor products.

Computational Method: The XMG-PDep Algorithm

XMG-PDep is based upon XMG [5], which developed from NetGen [6]. It employs flux-based termination of the otherwise combinatorial growth in species and reactions. To do this, the code periodically constructs and integrates the set of differential equations that represent the evolution of the reacting system in time. It evaluates a characteristic mechanism flux $R_{char}(t)$, which is similar to a root-mean-square average of chemical fluxes in the mechanism [7]. XMG-PDep then compares this flux with those to candidate species that have been discovered, but not yet included, in the mechanism. Those species whose fluxes exceed the cutoff flux (equal to a user-specified fraction of $R_{char}(t)$) are included in the mechanism and their reactions are explored, to generate new candidates. Eventually, all fluxes to candidate species are below the threshold $R_{char}(t)$ and generation is terminated.

XMG-PDep can systematically discover and include arbitrary pressure-dependent reactions using the algorithm of ref. [8]. To allow the most flexibility, XMG-PDep considers any elementary step of the form $A + B \rightarrow C$, $B \rightarrow C$ or $B \rightarrow C + D$ to initiate a partial pressure-dependent network. For each partial network, XMG-PDep uses the QRRK/MSM code CHEMDIS [9] to estimate the value of the pressure-dependent rate constant $k(T,P)$ for every net pressure-dependent reaction. It also examines the maximum flux to all non-included portions of the partial pressure-dependent network. If this flux is greater than the cutoff flux, the partial network is “grown” by one isomer, with all its high-pressure-limit elementary steps, and the $k(T,P)$ calculation is repeated. Growth of each partial pressure-dependent network is halted when the flux to non-included portions is less than the cutoff flux. In this way pressure-dependent reactions can be included systematically and rationally. A full description of the integrated algorithm for generating mechanisms is presented in ref. [3].

XMG-PDep includes a number of other features designed to make it accurate and useful. It employs literature-based libraries of rate constants and thermochemical parameters whenever possible. Its rate rules are subdivided as much as is reasonable to provide the best estimates for high-pressure-limit rates when these are not available from the library. Thermochemical data (when not available from the data library) are taken from a group contribution method [9] and used to ensure thermodynamic reversibility. The code will produce a CHEMKIN-style mechanism when finished with generation. Finally, we have recently added to XMG-PDep two new capabilities essential for treating the Glasier and Pacey system: an internal plug-flow reactor model to overcome the batch reactor restriction, and an ability to construct mechanisms spanning a temperature range.

Application to High-Conversion Ethane Pyrolysis

Figures 1-3 present selected predictions of our generated model along with experimental results. Agreement with the data is quite good, considering that no parameters were adjusted to fit the experiments, thermodynamic consistency is enforced, and all steps in the mechanism are generated “a priori”.

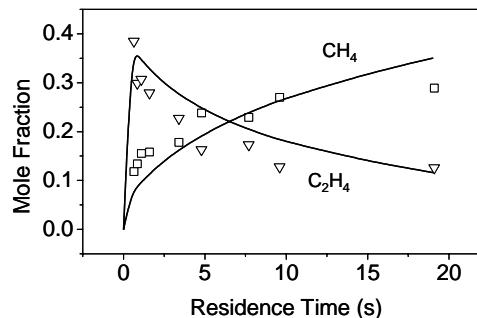


Figure 1. CH₄ and C₂H₄ concentrations with residence time in the Glasier and Pacey flow reactor. Symbols are experimental data points; lines are auto-generated model predictions.

Reaction pathway analysis, shown in simplified form in Figures 4 and 5, of the very large mechanism generated for this system suggests that the fates of the minor products, and some major ones, are governed in part by a large and complex set of interconnected reactions. Conventional kinetic models for ethane or ethylene pyrolysis do not capture many of these pathways.

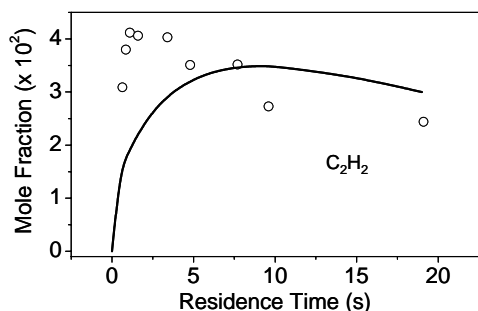


Figure 2. Experimental and predicted acetylene concentration with residence time.

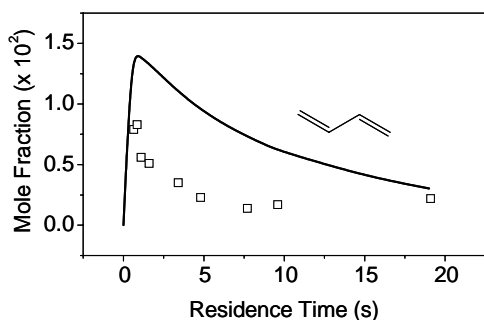


Figure 3. Experimental and predicted 1,3-butadiene concentration with residence time.

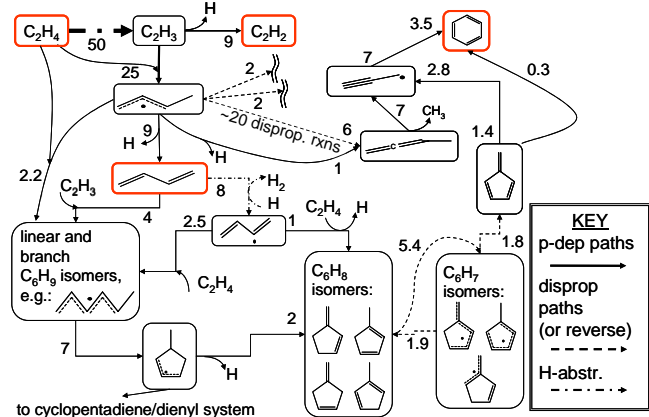


Figure 4. Partial pathway diagram for the production and consumption of minor products within the reactor “hot zone” (from 7.5 to 30 cm). Each arrow represents a collection of parallel, reversible reaction pathways of the same general type: solid lines are net pressure-dependent pathways; dotted lines are radical disproportionation reactions; dash-dotted lines are radical abstraction reactions. Numbers represent integrated, net molar flux relative to C₂H₄ consumption (= 100).

A key feature in Figures 4 and 5 is the presence of multiple, interconnected routes to the important minor products. There are at least three routes to benzene, four routes for the formation of propylene, and two alternatives to the well-known vinyl radical beta scission route for acetylene formation. Many of these pathways are pressure-dependent at the experimental conditions. Sensitivity analyses confirm the overall view that vinyl radical addition to ethylene to form the resonantly-stabilized allylic butenyl radical is a

key rate limiting step for both 1,3-butadiene and benzene formation, as has been alluded by Roscoe et al [10].

Another unusual feature of the model is the set of radical disproportionation reactions which generate 1,2-butadiene – the 1,2-butadiene yields propargyl radicals which combine to form benzene (Figure 4). No single reaction in this set of 20 is important enough, by itself, to be noticeable during sensitivity analysis. Our a priori effort suggests, however, that the aggregate affect of the pathways could be quite important.

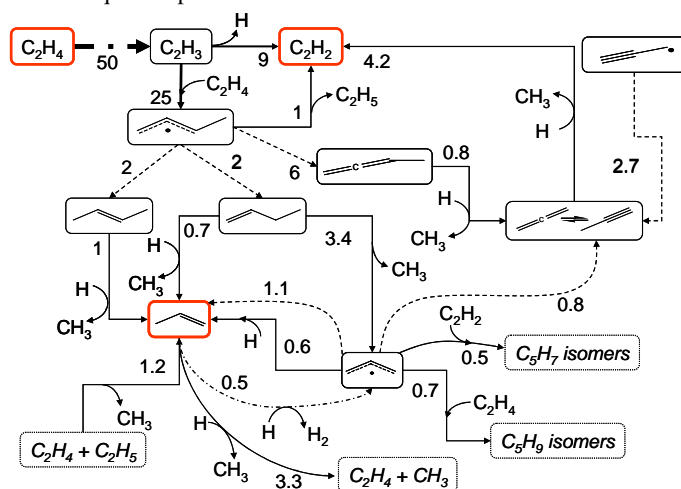


Figure 5. Continuation of Figure 4.

Conclusions

Application of the XMG-PDep algorithm to the experimental system of Glasier and Pacey yields a systematic kinetic model which appears to describe the gas-phase chemistry. This a priori model may prove useful as a base for advancing the mechanistic understanding of aromatics and pyrocarbon formation. Although complex, the generated model affords an understanding of the rate-limiting steps and pathways to the measured minor products in this system, such that changes in their behavior with temperature and pressure can be predicted (as is planned for future work). XMG-PDep explores many pathways not usually considered in other pyrolysis systems, and finds certain sets of reaction pathways, such as radical disproportionations, which might elude by-hand model construction.

References

- (1) Oberlin, A. *Carbon* **2002**, *40*, 7-24.
- (2) Glasier, G. F.; Pacey, P. D. *Carbon* **2001**, *39*, 15-23.
- (3) Matheu, D. M. *Integrated Pressure-Dependence in Automated Mechanism Generation: A New Tool for Building Gas-Phase Kinetic Models*, Ph.D. Thesis, Massachusetts Institute of Technology, **2002**.
- (4) Matheu, D. M., Dean, A. M., Grenda, J. M., and Green, W. H. Jr. *J. Phys. Chem.*, submitted for publication.
- (5) Grenda, J. M.; Androulakis, I. P.; Dean, A. M.; Green, W. H. Jr. *Ind. Eng. Chem. Res.* **2003**, *42*, 1000-1010.
- (6) Susnow, R. G.; Dean, A. M.; Green, W. H.; Peczek, P.; Broadbelt, L. *J. J. Phys. Chem. A* **1997**, *101*, 3731-40.
- (7) Song, J.; Stephanopoulos, G.; Green, W. H. *Chem. Eng. Sci.* **2002**, *57*, 4475-4491.
- (8) Matheu, D. M.; Lada, T. A.; Green, W. H.; Grenda, J. M.; Dean, A. M. *Comp. Phys. Comm.* **2001**, *138*, 237-249.
- (9) Chang, A. Y.; Bozzelli, J. W.; Dean, A. M. *Z. Phys. Chem.* **2000**, *214*, 1533-1568.
- (10) Roscoe, J. M.; Bossard, A. R.; Back, M. H. *Can. J. Chem.* **2000**, *78*, 16-25.